Available online at www.sciencedirect.com

ScienceDirect

Advances in Space Research 74 (2024) 5991–6011

ADVANCES IN SPACE RESEARCH
(a COSPAR publication)

www.elsevier.com/locate/asr

A review of global long-term changes in the mesosphere, thermosphere and ionosphere: A starting point for inclusion in (semi-) empirical models

Ingrid Cnossen [a,*], John T. Emmert [b], Rolando R. Garcia [c], Ana G. Elias [d], Martin G. Mlynczak [e], Shun-Rong Zhang [f]

[a] British Antarctic Survey, High Cross, Madingley Road, Cambridge CB3 0ET, United Kingdom
[b] Space Science Division, U.S. Naval Research Laboratory, Washington, DC, USA
[c] National Center for Atmospheric Research, Boulder, CO, USA
[d] Facultad de Ciencias Exactas y Tecnologia (FACET), Universidad Nacional de Tucuman (UNT) & INFINOA (CONICET-UNT), Tucuman 4000, Argentina
[e] NASA Langley Research Center, Hampton, VA, USA
[f] MIT Haystack Observatory, Westford, MA, USA

Received 20 August 2024; received in revised form 1 October 2024; accepted 4 October 2024
Available online 10 October 2024

Abstract

The climate of the upper atmosphere, including the mesosphere, thermosphere and ionosphere, is changing. As data records are much more limited than in the lower atmosphere and solar variability becomes increasingly dominant at higher altitudes, accurate trend detection and attribution is not straightforward. Nonetheless, observations reliably indicate that, on average, the mesosphere has been cooling, the density in the thermosphere has been decreasing, and ionospheric layers have been shifting down. These global mean changes can be largely attributed to the increase in CO_2 concentration, which causes cooling and thermal contraction in the middle and upper atmosphere. The decline in thermosphere density is particularly relevant from a practical viewpoint, as this reduces atmospheric drag and thereby increases orbital lifetimes and the build-up of space debris. Long-term changes in the ionosphere can have further practical implications and are not only driven by the increase in CO_2 concentration, but also by changes in the Earth's magnetic field. The empirical models that are mostly used to inform applications in industry on the state of the upper atmosphere, as well as being widely used in science, do not yet properly account for long-term trends in the mesosphere, thermosphere and ionosphere. This is problematic when long-term future projections are needed or models rely strongly on older data. This review provides an overview of the main evidence of long-term trends observed in the mesosphere, thermosphere and ionosphere, together with the latest insights on what causes these trends. It is hoped that this may serve as a starting point to include long-term trends in (semi-) empirical models to benefit all users of these models. We also offer some thoughts on how this could be approached.

Keywords: Mesosphere; Thermosphere; Ionosphere; Long-term trend

1. Introduction

Climate change is taking place throughout the atmosphere, from the surface up to the edge of space. The state of the upper atmosphere is increasingly important for the

* Corresponding author.
E-mail address: inos@bas.ac.uk (I. Cnossen).

https://doi.org/10.1016/j.asr.2024.10.005
0273-1177/© 2024 COSPAR. Published by Elsevier B.V.

management of the large number of satellites operating in this environment, and its long-term sustainability is a growing concern (e.g., Boley and Byers, 2021; Mlynczak et al., 2021; Shutler et al., 2022). One serious worry is the observed long-term decline in the density of the thermosphere (e.g., Keating et al., 2000; Emmert, 2015; Weng et al., 2020) and its impact on the space debris population. Objects orbiting within the thermosphere experience atmospheric drag, which is proportional to the ambient density. Atmospheric drag is the main mechanism by which space debris is removed from the Low Earth Orbit (LEO) environment (∼200–2000 km altitude), so that the long-term reduction in thermosphere density leads to a longer lifetime and more rapid increase in the amount of debris, increasing the risk of collisions with active satellites (Lewis et al., 2011; Brown et al., 2021). Satellite mission planning must also take the long-term effects on predicted orbits into account. Long-term changes in the ionosphere, the charged portion of the upper atmosphere, have additional practical implications (e.g., Danilov and Berbeneva, 2021). The total electron content (TEC) in the ionosphere is important for Global Navigation Satellite Systems (GNSS) signal propagation and any applications that require ionospheric corrections and long-term measurement stability, such as sensitive climate monitoring of sea level changes. Such applications require a good understanding of climatic changes in TEC to avoid spurious long-term signals in satellite-based data products (Scharroo and Smith, 2010).

Empirical or semi-empirical models such as the Mass Spectrometer Incoherent Scatter radar (MSIS) model series (Emmert et al., 2020; Emmert et al., 2022), the Drag Temperature Model (DTM)-2020 (Bruinsma and Boniface, 2021), the Jacchia-Bowman (JB2008) model (Bowman et al., 2008), and the International Reference Ionosphere (IRI) (Bilitza et al., 2022) are widely used in science and engineering, but for the most part these do not currently include a long-term trend component. That means that they may perform well for the period covered by the data they rely on, but are likely to accumulate biases as they are applied to periods further into the future. This could become problematic for many practical and scientific applications. To address this problem, first of all, a solid understanding of climate change at all levels and within all regions of the atmosphere is important. Here we will focus on the mesosphere, thermosphere, and ionosphere, which we also collectively refer to as the upper atmosphere.

While the troposphere shows a global mean warming trend, the middle and upper atmosphere have experienced a global mean cooling (e.g., Laštovička et al., 2006a), primarily attributed to the increase in carbon dioxide (CO_2) concentration (Laštovička et al., 2006a; Laštovička, 2017; Qian et al., 2011; Qian et al., 2021; Cnossen, 2012; Cnossen, 2020). CO_2 absorbs and re-emits infrared radiation at 15 μm. Near the surface, this leads to a net warming, which is communicated to the rest of the troposphere via convection. However, infrared emissions are mostly lost to space, resulting in net cooling above the tropopause (Manabe and Wetherald, 1967; Manabe and Wetherald, 1975; Roble and Dickinson, 1989). Mlynczak et al. (2024) demonstrated that the same amount of energy is radiated over time, but as CO_2 levels rise, this happens at a lower equilibrium temperature. Above ∼130 km altitude, the CO_2 concentration becomes so small that it no longer directly affects the local temperature through radiative processes; instead infrared cooling by nitric oxide (NO) and atomic oxygen becomes more important (see Fig. 1). However, heat conduction additionally transports energy from the middle and upper thermosphere down to the lower thermosphere, where it can be radiated by CO_2 (e.g., Mlynczak et al., 2022). Mlynczak et al. (2018) called this the "heat sink region". When the lower thermosphere is cooler, the vertical temperature gradient in the thermosphere increases, resulting in more effective heat conduction, so that enhanced CO_2 levels indirectly lead to a cooler thermosphere as a whole. Increases in the concentration of other greenhouse gases, such as methane (CH_4), and water vapour (H_2O), as well as the reduction in stratospheric ozone (O_3) concentration are additional contributors to cooling trends in the stratosphere and mesosphere (Akmaev et al., 2006; Garcia et al., 2007; Lübken et al., 2013), but their role decreases with increasing altitude and becomes very small or even negligible in the upper thermosphere (Qian et al., 2013; Qian et al., 2014). Quantifying the role of ozone is further complicated by its non-uniform temporal variation: before ∼1980 the ozone concentration was relatively constant, followed by a strong decline until the mid-1990s, and a gradual recovery in more recent years (Harris et al., 2015; Weber et al., 2022). The relative importance of long-term changes in ozone concen-

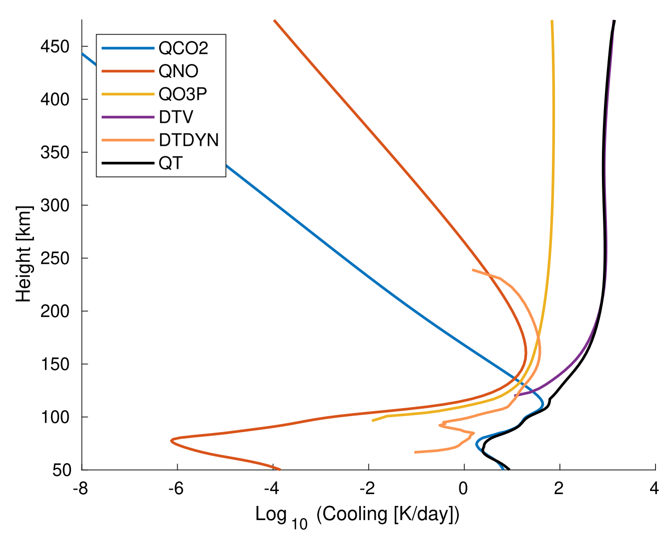

Fig. 1. Global mean annual mean infrared cooling rates due to CO_2 (QCO2), NO (QNO), and atomic oxygen (QO3P), cooling due to downward heat conduction (DTV), cooling due to resolved dynamics and parameterized gravity waves (DTDYN) and the total heating rate (QT) calculated from a Whole Atmosphere Community Climate Model - eXtended (WACCM-X) simulation (https://doi.org/10.26024/5b58-nc53) using data for 2018.

tration, and even the sign of the effect, is therefore strongly dependent upon the time frame under consideration.

A key side effect of the global cooling of the middle and upper atmosphere is thermal contraction: as the atmosphere cools, it shrinks. Thermal contraction causes a downward shift of constant pressure levels and the associated temperature, neutral density, and electron density structures. It is responsible for the observed decline in thermosphere density and also causes fundamental atmospheric features, such as the mesopause or the peak of the ionospheric F_2 layer, to move down. In addition, thermal contraction can lead to quite different vertical profiles of long-term trends evaluated in constant height versus constant pressure reference frames (e.g., Akmaev and Fomichev, 1998). Not only can this cause considerable differences in trend magnitude, it can even result in differences in sign, as illustrated in Fig. 2 for the global mean temperature. The choice of reference frame has the largest impact in the upper mesosphere and lower thermosphere, where the vertical temperature gradient is large. In a constant height reference frame, an apparent heating can be found here, due to the downward shift of the entire temperature profile. This causes, for instance, the lower thermosphere to move into what was formerly the (colder) upper mesosphere. In contrast, a constant pressure reference frame shows cooling throughout. One should therefore be clear about the reference frame used when reporting long-term trends in the upper atmosphere.

For the ionosphere in particular, there is a further complicating element: the secular variation of the Earth's magnetic field. Over the past ~100 years, the magnetic dipole moment has decreased by about 6–6.5%, while the magnetic dip poles and magnetic equator have been moving northwestward (Finlay et al., 2010; Alken et al., 2021).

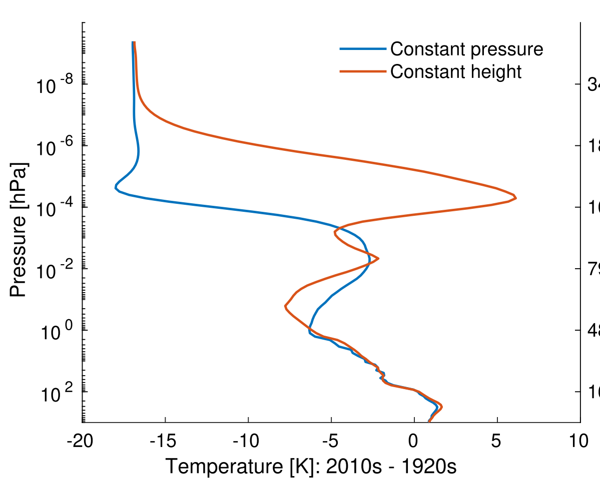

Fig. 2. Global mean multi-annual mean difference in neutral temperature between the 2010s (2010–2015) and the 1920s (1920–1925) evaluated in constant pressure (blue) and constant height (orange), calculated from WACCM-X simulations by McInerney et al. (2024), available at https://doi.org/10.5065/w3x2-fz18. (For interpretation of the references to colour in this figure legend, the reader is referred to the web version of this article.)

The strongest changes in the magnetic field have occurred over South America and the southern Atlantic Ocean due to the westward movement, expansion and deepening of the South Atlantic Anomaly (SAA), a region of weak magnetic field intensity. Changes in the strength and orientation of the magnetic field cause widespread changes in the ionosphere, including changes in conductivity, plasma transport, peak electron density, total electron content, and the general spatio-temporal structure of the ionosphere and ionospheric current systems (Takeda, 1996; Yue et al., 2008; Cnossen and Richmond, 2008; Elias, 2009; Gromenko et al., 2012; Cnossen and Richmond, 2013; Zhang and Holt, 2013; Cnossen, 2014; Tao et al., 2017; Wang et al., 2017; Zossi et al., 2018; Cai et al., 2019; Cnossen and Maute, 2020; Qian et al., 2021; Elias et al., 2022; Wang et al., 2022). Locally, magnetic field changes can even affect the neutral upper atmosphere, e.g., the thermosphere temperature (Cnossen, 2014; Cnossen, 2020; Cnossen et al., 2016), density (Wang et al., 2017), or winds (Cnossen et al., 2016; Wang et al., 2022). However, magnetic field-induced changes in both the ionosphere and thermosphere are strongly location-dependent, often showing negative changes in some regions, compared to positive changes in others, which largely cancel out in global averages (Cnossen, 2014; Qian et al., 2021). Nonetheless, it is important to take magnetic field effects into account when evaluating local long-term trends that may be affected by these (e.g., Elias and de Adler, 2006a; de Haro Barbas et al., 2013; Gnabahou et al., 2013; Shinbori et al., 2014; Cnossen and Matzka, 2016; Thu et al., 2016; Matzka et al., 2017; Yue et al., 2018; Soares et al., 2020; Slominska et al., 2020).

Another factor that must be considered is the effect of solar and geomagnetic activity variations. Solar extreme ultraviolet (EUV) radiation is the main source of heating and ionization in the middle and upper atmosphere, with geomagnetic activity providing a further source of heating and ionization, in particular at high latitudes (e.g., Roble, 1995; Schunk and Nagy, 2000). As a result, the variation induced by the approximately 11-year solar cycle is much larger than any underlying long-term trends, which makes it difficult to extract these trends reliably from observational records. As a minimum requirement to do this successfully, data records need to span several solar cycles and ideally they should start and end at comparable solar activity levels (Clilverd et al., 2003; Laštovička and Jelínek, 2019). Most trend analysis methods then rely on solar proxies, such as the sunspot number, 10.7 cm radio flux (F10.7), 30 cm radio flux (F30), or Mg II core-to-wing ratio, to filter out solar activity influences and calculate the long-term trend from the data. However, no proxy is perfect and the choice of solar proxy can affect the trend obtained (Laštovička et al., 2006; Mielich and Bremer, 2013; de Haro Barbás et al., 2021; Laštovička, 2021b). While recent studies indicate that F30 may be the best proxy to use for thermosphere density modelling (Dudok de Wit and Bruinsma, 2017) and ionospheric peak electron density trend analysis (Laštovička, 2021a; Laštovička, 2024), previous studies have used a variety of solar proxies and this is likely to be a source of discrepancy among them. Another point in this regard is that the relationships between solar proxies, actual EUV emissions and upper atmosphere parameters may not remain constant over time (Lukianova and Mursula, 2011; Bruevich and Bruevich, 2019; Laštovička, 2019; Mursula et al., 2024), which can also affect the trends obtained (Elias, 2014; Elias et al., 2014; de Haro Barbas and Elias, 2015; Laštovička et al., 2016; Danilov and Konstantinova, 2020; Mlynczak et al., 2022). Further, there may be long-term (non-cyclical) trends present in solar EUV emissions (Matthes et al., 2017) and geomagnetic activity levels (Clilverd et al., 1998; Clilverd et al., 2005; Stamper et al., 1999; Lockwood et al., 1999), depending on the time window studied, which can contribute to trends in middle and upper atmosphere parameters and the associated effects induced by thermal contraction/expansion. These are difficult to disentangle from CO_2-induced effects (Cnossen and Franzke, 2014; Emmert, 2015). An additional problem is that the background solar activity level is thought to modulate the effect of CO_2-induced trends in the thermosphere due to its influence on cooling rates from other minor species, in particular nitric oxide (NO) (Solomon et al., 2019; Lin and Deng, 2019). NO cooling is much more sensitive to the background temperature than CO_2 cooling (e.g., Mlynczak et al., 2010), so that CO_2 cooling in the lower thermosphere becomes relatively less important at solar maximum, which is expected to result in smaller CO_2-induced trends at solar maximum (e.g., Qian et al., 2006; Qian et al., 2011). For all these reasons, accounting for solar and geomagnetic activity effects as part of long-term trend analysis in the middle and upper atmosphere is not a trivial task. The deep and prolonged solar minimum of 2008/2009 (Lockwood, 2010; Russell et al., 2010) poses a particularly hard challenge for trend analysis (e.g., Emmert et al., 2014; Emmert, 2015; Emmert et al., 2017), as the unusually low activity levels are not necessarily captured well by the solar activity indices commonly used for trend analysis (e.g., Solomon et al., 2013) and can lead to unrealistic trends (e.g., Elias et al., 2014; Danilov and Konstantinova, 2016).

Other obstacles for reaching a consistent global, quantitative description of long-term changes in the upper atmosphere include: 1) the relatively sparse amount of data that is available, at least compared to the amount of data available to study climate change in the lower atmosphere; 2) differences in data coverage, both in time and space, offered by different kinds of data sets (e.g., local, ground-based measurements versus satellite observations); and 3) differences in analysis methods. Most long-term trend analyses in the middle and upper atmosphere rely on some form of (multi-) linear regression to filter out non-trend components from the data and determine the trend itself (e.g., Laštovička and Jelínek, 2019), but more recently, artificial intelligence (AI) methods have been more commonly used as well (e.g., Yue et al., 2006; Cai et al., 2019; Weng et al., 2020). All this must be borne in mind when evaluating long-term trends determined from observational records in the middle and upper atmosphere.

In this review we will summarize the observational evidence for long-term changes in the mesosphere, thermosphere and ionosphere, including uncertainties and discrepancies that have not yet been resolved. Relevant modelling results that provide insights on what has caused these changes will also be discussed. The goal is to provide a basis from which these long-term changes can start to be included in (semi-) empirical models. Since CO_2 plays a dominant role in driving long-term trends in the upper atmosphere, we will first review the evidence on trends in the atmospheric CO_2 concentration itself, with emphasis on the mesosphere and lower thermosphere. The following sections will then discuss long-term trends in the mesosphere, mesopause region, thermosphere, and ionosphere. Section 7 provides a forward look on trends that we can expect in the future and some thoughts on how long-term trends might be incorporated into empirical models. We finish with a brief summary and conclusions.

2. Carbon dioxide

The CO_2 concentration is approximately invariant with height up to ~80 km as a result of atmospheric vertical mixing. Above 80 km, the CO_2 mixing ratio decreases with increasing altitude as a result of vertical diffusion relative to lighter species and due to photolysis. The concentration of CO_2 in the troposphere is currently increasing at a rate of ~25 ppm/decade (Dr. Xin Lan, NOAA/GML (gml.noaa.gov/ccgg/trends/) and Dr. Ralph Keeling, Scripps Institution of Oceanography (scrippsCO2.ucsd.edu/)). This corresponds to a relative trend of ~5–6% per decade. It is generally assumed that the relative trend propagates upward via vertical mixing processes, such that it should be approximately invariant with height. Simulations with the Whole Atmosphere Community Climate Model (WACCM) in principle confirm this (e.g., Yue et al., 2015). However, this assumption has only recently been tested against observations, mainly using satellite-based measurements from the Atmospheric Chemistry Experiment Fourier Transform Spectrometer (ACE-FTS) and the Sounding of the Atmosphere using Broadband Emission Radiometry (SABER) instrument. ACE-FTS measures solar occultation infrared spectra, from which the concentrations of numerous species, including CO_2 and CO, are derived, while SABER CO_2 concentrations are derived from measurements of 4.3 μm and 15 μm airglow emissions.

Yue et al. (2015) used SABER measurements from 2002 to 2014 to calculate CO_2 trends in the 65–110 km altitude range. Below 80 km, they estimated a ~5% per decade relative trend, consistent with the measured tropospheric trend. However, above ~90 km, their trend estimates increased with altitude, with a value of ~8% ± 2% per decade near 100 km altitude. Emmert et al. (2012) found comparably large trends around 100 km altitude based on ACE-FTS data.

Emmert et al. (2012) initially suggested that the large observed CO_2 trend around 100 km altitude might be caused by an increase in vertical mixing, which would draw more CO_2 to higher altitudes. However, Garcia et al. (2016) noted there is no observational evidence for a trend in vertical mixing large enough to explain the discrepancy between the observed trend in CO_2 concentration and the WACCM-based trend around 100 km altitude. Qian et al. (2017) instead showed that at least some of the discrepancy could be ascribed to methodology and data quality issues when analyzing the SABER and ACE-FTS data, respectively. In contrast to the earlier studies, they obtained trends near 96 km altitude of 5.1% per decade from both datasets, consistent with the tropospheric trend and WACCM (see Fig. 3). For ACE-FTS, the reduction in trend magnitude arose from the use of a newer version (3.5 versus 3.0 used by Emmert et al. (2012)), which included more detailed quality flags. By excluding observations with any kind of an adverse quality flag assigned, Qian et al.

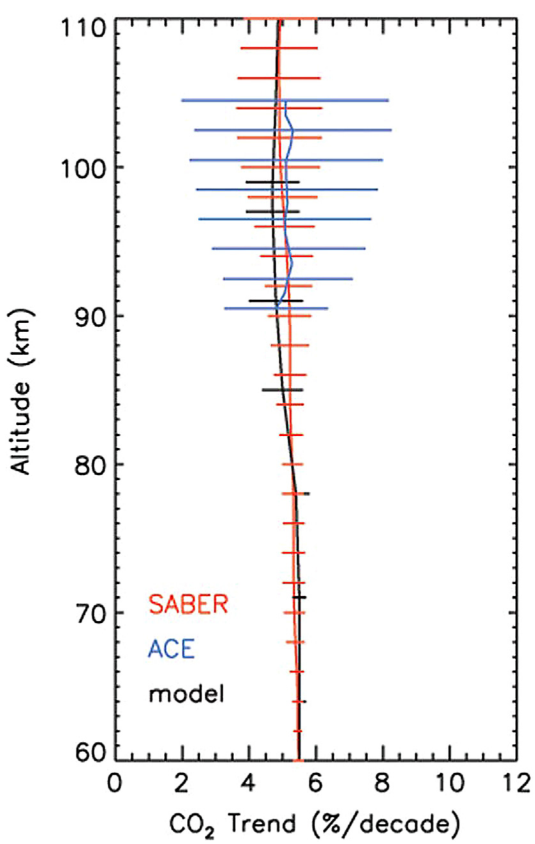

Fig. 3. Vertical profiles of the relative CO_2 trends in %/decade in altitude coordinates, obtained from SABER (red), ACE-FTS (blue) and WACCM (black). The horizontal bars indicate the trend estimation uncertainty at each vertical level. From Qian et al. (2017). (For interpretation of the references to colour in this figure legend, the reader is referred to the web version of this article.)

(2017) obtained smaller trends. For SABER, they found that the previously inferred trends by Yue et al. (2015) were sensitive to the temporal bin size used as part of their deseasonalization method. Rezac et al. (2018) showed that the nonuniform spatial and temporal sampling (particularly local time sampling) of SABER is responsible for this sensitivity. They warned that using monthly averages can lead to an overestimated linear trend and recommended a 60-day SABER binning for trend studies to provide more uniform local time sampling. This also applies to other variables observed by SABER. Liu et al. (2024) argued that a binning based on the SABER yaw cycle, which varies between 54 and 64 days, would be even better, in combination with a correction for seasonal variations. Qian et al. (2017) additionally found that ACE and SABER CO_2 trends between 90 and 105 km are slightly larger when calculated in pressure coordinates than when calculated in altitude coordinates. With the recommended methodology and calculating trends in pressure coordinates, Rezac et al. (2018) obtained relative CO_2 trends that do not differ significantly from WACCM, or from the tropospheric trend, below ~90 km. However, above 90 km, their relative SABER trends still increased with altitude to a maximum of ~8% per decade around 105–110 km altitude.

Pramitha et al. (2023) offer the most recent analysis of SABER CO_2 trends. Using data for 2002–2017, they applied multi-linear regression analysis directly to 60-day averages of the data (overlapping at 1 month intervals) in 5° latitude bins from 50°S to 50°N. Their formulation included a linear trend, annual (but not semiannual) harmonics and a linear solar activity term in F10.7, as well as terms for the Quasi-Biennial Oscillation (QBO) and El Niño Southern Oscillation (ENSO). Between 40 and 90 km altitude, they obtained a CO_2 relative trend of 4.5–4.7% per decade, increasing to 5–7% per decade above 95 km, with no noted latitude dependence. Pramitha et al. (2023) also calculated trends from a thermospheric extension of WACCM (WACCM-X), obtaining trends of 1.5–2% per decade at 40–100 km altitude, which is much smaller than observed and smaller than the WACCM trends obtained in earlier studies. However, this result must be due to an error in the WACCM-X simulation used by Pramitha et al. (2023) (see note at https://www2.hao.ucar.edu/sites/default/files/2022-10/sd_waccmx_co2.pdf).

Overall, the current observational evidence indicates that the CO_2 concentration is increasing in the mesosphere and lower thermosphere at the rate of 5–7% per decade. Given that there is likely an uncertainty of around 1–2% per decade, this is statistically consistent with model predictions, which indicate that relative trends are 4.5–5.5% per decade throughout the atmosphere up to 110 km and largely independent of altitude. As the temporal length of the observational record increases (ACE and SABER are currently still operational), it may be possible to reduce the statistical uncertainty of the trend estimates to detect any altitudinal or latitudinal dependencies therein.

3. Mesosphere

In the past, only limited, local information on long-term trends in the temperature in the mesosphere has been available. Beig et al. (2003) and Beig (2011) reviewed many studies based on rocketsonde and lidar measurements, indicating that the mesosphere has been cooling since the 1970s, at a rate of around −1 to −3 K/decade. More recent lidar studies more or less confirm this, although trend magnitudes vary considerably among stations, from no significant trend to as much as −4 K/decade (Li et al., 2011; Kishore et al., 2014). This may reflect to some degree true spatial variations in trend magnitude, but it is likely that differences in the period analysed and differences in analysis techniques also play a role.

Satellite data offer better spatial coverage and can help to establish a more comprehensive picture of mesospheric cooling, although they are only available for the last few decades. To obtain a sufficiently long data record for trend analysis, Li et al. (2021) combined observations from the Halogen Occultation Experiment (HALOE) instrument (1991–2005) and the SABER instrument (2002–2019). Fig. 4 shows they found cooling trends throughout the mesosphere between 45°S and 45°N up to 80 km, maximising in the southern hemisphere (SH) tropical and subtropical region at 60–70 km altitude at about −1.2 K/decade, with slightly weaker cooling in the northern hemisphere (NH).

Bailey et al. (2021) also used HALOE and SABER data, as well as data from the Solar Occultation for Ice Experiment (SOFIE) instrument, but concentrated on trends during summer at 64–70° in both hemispheres (June in NH; December in SH). They showed noticeably stronger mesospheric cooling trends, up to about −2 K/decade in the SH, with again slightly weaker cooling in the NH. Bailey et al. (2021) also showed evidence of the thermal contraction caused by mesospheric cooling in the form of a downward shift of constant pressure surfaces of around −100 to −200 m/decade. These results are shown in Fig. 5. However, we note that Bailey et al. (2021) used monthly means in their analysis and for SABER this has been shown to lead to an overestimation of trends when a strong diurnal cycle is present (Rezac et al., 2018). Although Bailey et al. (2021) do not rely solely on SABER data, it is possible that their trends are too large as a result. On the other hand, it is also possible that the cooling trends truly are larger at higher latitudes, perhaps due to dynamical effects. At high latitudes during summer (and winter), adiabatic cooling is an important part of the heat budget, so that temperature trends could be influenced by changes in upwelling, rather than being purely radiatively driven, as would be expected at low to mid-latitudes. We further note that Li et al. (2021) reported trends in constant height, whereas Bailey et al. (2021) used a constant pressure reference frame, which is another difference between these studies. However, as temperature trends in the mesosphere (in the ~50–90 km height range) should generally appear larger

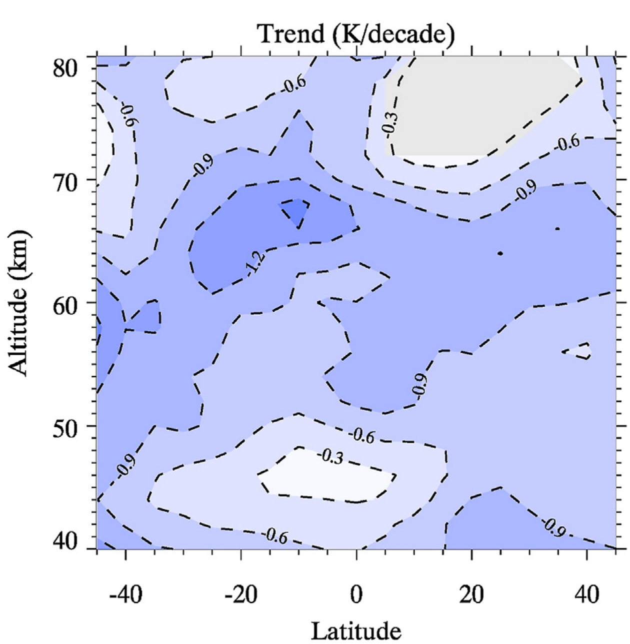

Fig. 4. Long-term temperature trend (K/decade) at 40–80 km from 45°S to 45°N derived from merged HALOE and SABER data (1991–2019). Blue colors represent negative trends with contour line intervals of 0.3 K/decade. The grey areas represent a significance level below 95%. From Li et al. (2021). (For interpretation of the references to colour in this figure legend, the reader is referred to the web version of this article.)

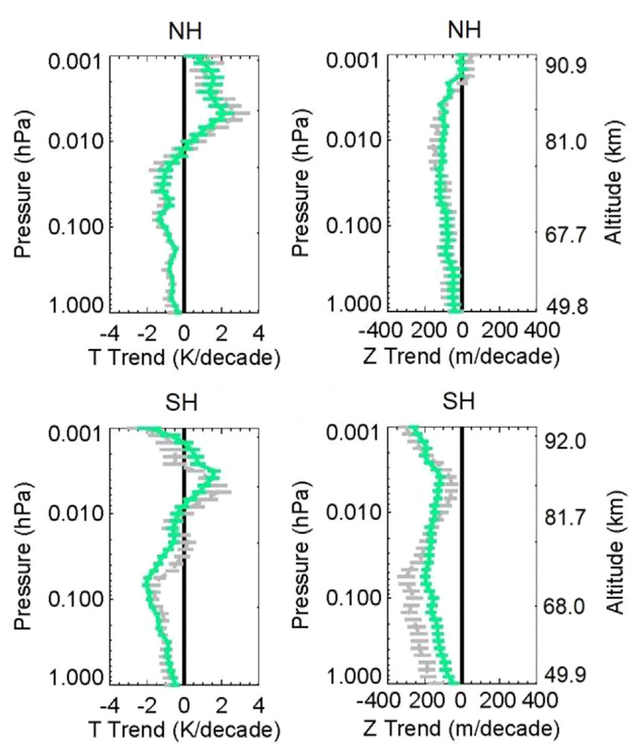

Fig. 5. Long-term trend in temperature (left) and pressure altitude (right) based on HALOE/SABER (green) and HALOE/SOFIE (grey) at 64–70° latitude in the NH (top) and SH (bottom) during local summer. From Bailey et al. (2021). (For interpretation of the references to colour in this figure legend, the reader is referred to the web version of this article.)

in a constant height reference frame (see Fig. 2; also Akmaev and Fomichev, 1998), this cannot explain why Bailey et al. (2021) found larger trends than Li et al. (2021).

Several studies analyzed only SABER data for long-term trends, even though the data records are still on the short side for this. Das (2021) and Zhao et al. (2021) did their analysis for 50°S-50°N, based on data from 2003–2019 and 2002–2020, respectively, while Mlynczak et al. (2022) analyzed a slightly larger latitude range, 55°S-55°N, based on data from 2002–2019. Despite using different analysis techniques (Das (2021) used Empirical Mode Decomposition (EMD), while Zhao et al. (2021) and Mlynczak et al. (2022) used standard multi-linear regression), they found similar mesospheric cooling trends of on average around −0.5 to −0.7 K/decade. These trends are a little weaker than those reported by Li et al. (2021) for a similar latitude range. Mlynczak et al. (2022) also reported a downward shift in the geopotential height of pressure levels in the mesosphere, from -47 ± 13 m/decade at 0.1 hPa to -127 ± 20 m/decade at 10^{-3} hPa. Zhao et al. (2021) showed no significant difference in average trend magnitude between the NH and SH at 10–50°, while Das (2021) only noted stronger cooling in the SH than the NH in certain regions. We conclude that it is not yet clear whether there is a true, systematic hemispheric difference in trends in mesosphere temperature or not; more data and analysis will be required to determine this. However, given that CO_2 is well-mixed, there is no reason to expect any interhemispheric differences in radiatively driven temperature trends.

Satellite-based mesospheric cooling trends tend to be smaller (mostly between about −0.5 and −1 K/decade, or up to −2 K/decade at high latitude) than the range of estimates provided by rocketsonde and lidar studies (on average between −1 and −3 K/decade). Modelling studies indicate that mesosphere temperature trends can largely be explained by the increase in CO_2 concentration and changes in ozone concentration (Akmaev et al., 2006; Garcia et al., 2019; Ramesh et al., 2020). Garcia et al. (2019) investigated the differences in global mean temperature trends with WACCM for a range of 21-year periods from 1955 to 2095. Fig. 6, reproduced from Garcia et al. (2019), clearly demonstrates the additional cooling caused by the reduction in stratospheric ozone during 1975–1995, the period dominated by the growth of anthropogenic halogen emissions, which destroy stratospheric ozone. A strong peak in cooling around the stratopause occurs for 1975–1995, a feature absent for all other periods shown, which also results in relatively strong cooling in the lower to middle mesosphere during 1975–1995. This could explain why satellite-based estimates of mesospheric cooling, which are largely based on data from the last 20–30 years, are generally smaller than cooling estimates based on rocketsonde and lidar studies, which usually include older data, and are hence more affected by the decline in stratospheric ozone during the 1980s and early 1990s, especially in the lower part of the mesosphere.

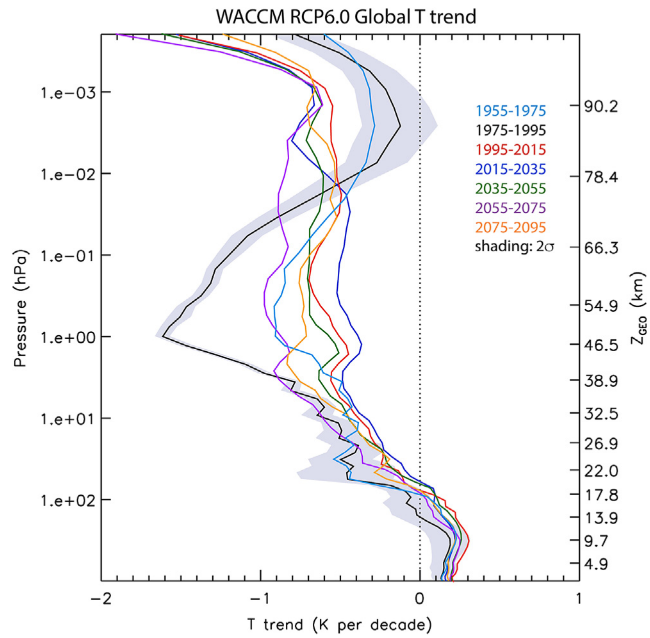

Fig. 6. Evolution of the global-mean temperature trend in the WACCM RCP6.0 scenario over 21-year periods spanning the second half of the twentieth century and all of the twenty-first century. Shading indicates the 2σ uncertainty range for the 1975–1995 trend but is representative also of other periods. From Garcia et al. (2019).

4. Mesopause region

4.1. Temperature

The reviews by Beig et al. (2003) and Beig (2011) reported that most studies at the time indicated or were consistent with there being no significant long-term temperature trend in the mesopause region (∼80–100 km), albeit with an uncertainty margin of at least 2 K/decade. More recently, significant trends have been reported, but with large differences dependent on location, season, and the period analysed (Offermann et al., 2010; Kalicinsky et al., 2016; She et al., 2019; Yuan et al., 2019; French et al., 2020). For example, Offermann et al. (2010) found an annual mean negative temperature trend of −2.3 K/decade at ∼87 km altitude based on 21 years of OH airglow measurements over Wuppertal (51°N, 7°E), but varying between 0 (no significant trend) and −6 K/decade for individual months. Kalicinsky et al. (2016) found a reversal in trend after 2008 at the same station after 7 more years of data were collected, with a trend of -2.4 ± 0.7 K/decade before 2008 and $+6.4 \pm 3.3$ K/decade after 2008. Such large differences in ”trend” indicate that any long-term changes, at least for this station, are very unstable, and we would argue that it is not actually helpful to refer to these numbers as ”long-term trends”. Furthermore, locally observed trends, even when they are reliable, may not necessarily be representative of the global picture. Satellite observations are essential to provide context.

French et al. (2020) analysed 14 years of Microwave Limb Sounder (MLS) data, showing trends ranging between about ±2 K/decade, depending on location and season, with zonal mean trends between −1 and +0.5 K/decade. An analysis of 18 years of SABER data by Zhao et al. (2020) showed consistently negative zonal mean trends, although these were not significant at all latitudes, with a global average mesopause temperature trend of -0.75 ± 0.43 K/decade. The analysis by Bailey et al. (2021), using data from the HALOE, SABER, and SOFIE instruments for 64–70° in both hemispheres during summer, extended up into the mesopause region. They showed that the cooling of around −1 to −2 K they found in most of the mesosphere reduces towards the mesopause and turns into a warming trend above 0.01 hPa (near 83 km altitude), peaking at around +2 K/decade in the NH and +1.5 K/decade in the SH (see Fig. 5). Bailey et al. (2021) also showed a downward shift in pressure surfaces in most of the mesopause region, except in the NH near 90 km altitude, where no clear trend was found. Liu et al. (2024) used SABER data (2002–2023) to analyze trends at 50°S-80°N and 80°S-50°N, depending on the season (or technically, the SABER yaw cycle). While they found considerable seasonal variations in mesopause temperature trends, on average the mesopause temperature is decreasing at all latitudes, with a trend of −0.3 to −1.0 K/decade at 50°S-50°N, increasing to around −1.0 to −1.5 K/decade at SH high latitudes and up to −2.0 to −2.5 K/decade at NH high latitudes. We note again that high-latitude temperature trends in particular are likely to be strongly influenced by changes in dynamics, which may or may not be secular. Further, Liu et al. (2024) warn that most of their mesopause temperature trends are not necessarily reliable as they tend to be smaller than the systematic trend uncertainty associated with SABER data. Nonetheless, the SABER-based trend estimates do seem in broad agreement with estimates based on other satellite instruments.

In addition, there is evidence of a downward trend in mesopause height from ground-based observations. Yuan et al. (2019) analyzed lidar observations at two mid-latitude stations, showing that the high mesopause above 97 km during non-summer months moves down at a rate of about 450 ± 90 m/decade, while the downward trend of the low mesopause below 92 km during non-winter months was much smaller and not significant. Dawkins et al. (2023) analyzed changes in the peak meteor ablation altitude observed by 12 meteor radars at different locations. This offers a measure of net atmospheric contraction between the mesopause region and the surface. They found an average trend of -396 ± 140 m/decade, but with considerable spatial variations, ranging from no significant trend to -818 ± 67 m/decade. The smallest altitude trends were found at low latitudes, with larger trends at mid-latitudes, and the largest variation at high latitudes.

4.2. Dynamics

In the mesopause region, analysis of just temperature timeseries may not be sufficient to fully understand the long-term trends, especially at high latitudes, where the atmosphere is far from radiative equilibrium and to a large extent dynamically controlled. In particular in the polar regions, the temperature is strongly affected by the large-scale gravity wave-driven circulation from the summer to winter pole. This results in upwelling and adiabatic cooling over the summer polar region and downwelling and adiabatic warming over the winter polar region. Any long-term changes in gravity wave activity, which might be expected to occur due to climatic changes in wave generation and/or wind filtering by the atmosphere below, would therefore likely affect temperature trends in the mesopause region (e.g., She et al., 2019). Modelling studies have also suggested dynamical changes occur as a result of increased CO_2 concentrations (e.g., Portmann et al., 1995; Akmaev and Fomichev, 1998; Schmidt et al., 2006). However, the observational evidence on long-term changes in winds and gravity wave activity in the upper mesosphere/lower thermosphere (MLT) region is limited.

Jacobi et al. (2015) found a strengthening of the zonal winds and a weakening of the meridional winds over Collm (52.1°N, 13.2°E), based on radar measurements from 1979 to 2008 near 90 km altitude. Jacobi (2014) reported mostly insignificant trends in gravity wave activity at the same station. Wilhelm et al. (2019) analyzed radar measurements from 2002 to 2018 for the high-latitude station Andenes (69.3°N, 16°E) and the mid-latitude stations Juliusruh (54.6°N, 13.4°E) and Tavistock (43.3°N, 80.8°W). All three stations showed different long-term trends in zonal and meridional winds, which were also dependent on season and height. The annual mean winds changed the most at Andenes, with the mean zonal wind speed decreasing by up to 3 m/s/decade and the meridional wind speed decreasing by up to 2 m/s/decade between 85 and 100 km altitude. At Juliusruh, the zonal wind only showed a weak long-term trend, while the meridional wind became more southward below 85 km altitude and more northward above. At Tavistock, a somewhat stronger northward trend was found above 90 km altitude, with no significant trend below and no significant trend in zonal wind either. Hoffmann et al. (2011) also examined radar measurements over Juliusruh, but studied long-term trends in gravity wave activity. They found a significant increase in summer gravity wave variances based on data from 1990 to 2010 at 84–88 km altitude.

Ratnam et al. (2013) combined rocketsonde (1977–1991), High Resolution Doppler Imager (HRDI) onboard the Upper Atmosphere Research Satellite (UARS) (1991–1999), and mesosphere-stratosphere-troposphere (MST) radar (1995–2010) data to construct a long-term data set of mesospheric winds (70–80 km altitude) over the Indian region from 1977 to 2010. They found a large weakening of the eastward wind of 20–30 m/s/decade, except during summer months. Ratnam et al. (2019) built on this data set by adding data from HALOE and SABER and confirmed a weakening of the strong eastward winds over the Indian region in the 1970s, changing to weak westward winds during the last decade, but at a slower rate of ~5 m/s/decade. No significant trends were observed in the meridional wind. Ratnam et al. (2019) reported good agreement with WACCM–X simulations, which included the effects of the increase in greenhouse gas concentrations (CO_2, CH_4 and H_20), as well as chlorofluorocarbon species that cause depletion of stratospheric ozone (O_3).

Liu et al. (2017) derived global gravity wave potential energy from 14 years of SABER data (2002–2015) and analyzed this data set for long-term trends. A significant positive trend of gravity wave potential energy at around 40–50°N was found throughout the mesosphere during July. This seems to be at least qualitatively consistent with Hoffmann et al. (2011). However, in most of the mesosphere, their trends were not significant. This does not necessarily mean that there really are (mostly) no significant long-term changes in mesospheric gravity wave activity; it is also possible that the variability in the data is too large to be able to detect trends accurately. Further, the solar activity influence is difficult to eliminate for such a short dataset, especially including the unusual solar minimum of 2008/2009, so that the results obtained are likely to be sensitive to the solar proxy used.

Both long-term trends in mean winds and in gravity wave activity appear to vary strongly with location and season. In addition, the data sets available are still relatively short for long-term trend analysis, especially given the large natural variability. We conclude that it is not yet possible to establish a reliable global picture of long-term changes in mean winds and gravity wave activity in the mesosphere. Collecting more data to extend the time-series and spatial coverage is needed to solve this problem.

5. Thermosphere

There are no sufficiently long measurement records available to analyse long-term trends in thermosphere temperature directly, except perhaps in the very lowest part of the thermosphere (below ~120 km altitude). Instead, thermospheric cooling is inferred from the long-term decline in thermosphere density, long-term trends in ion temperature, and the lowering of ionospheric layers. Evidence of long-term trends in thermosphere density and ion temperature trends will be discussed below, while the lowering of ionospheric layers will be treated in Section 6.

5.1. Density

Due to thermal contraction, the density at fixed heights in the thermosphere decreases, resulting in less atmospheric drag on objects orbiting within the upper atmosphere. As this manifests itself in the orbital trajectories, satellite orbit data have proved to be a valuable resource to estimate long-term trends in thermosphere density. The first study of long-term density trends by Keating et al. (2000) indicated a global mean decrease of -4.9 ± 1.3 %/decade at 400 km altitude under solar minimum conditions. Further studies that have been conducted since then (Emmert et al., 2004; Marcos et al., 2005; Emmert et al., 2008; Saunders et al., 2011; Emmert, 2015; Weng et al., 2020) have mostly reported somewhat smaller trends of around −1.5 to −3 %/decade (see review in the introduction of Emmert (2015) for details). There is general agreement that density trends increase slightly in magnitude with increasing height between 250 and 575 km altitude, as shown in Fig. 7, which is consistent with a cooling and contracting mesosphere and thermosphere.

Initial studies suggested that thermosphere density trends were larger for low background solar activity levels (Emmert et al., 2004; Emmert et al., 2008). However, more recent studies suggest that there is no significant solar activity dependence (Emmert, 2015; Weng et al., 2020), although the deep solar minimum of 2008/2009 does cause difficulties in trend estimation. Emmert (2015) estimated a density trend at 400 km altitude of -2.0 ± 0.5 %/decade between 1967 and 2005, but the estimated density trend increased with more recent data up to 2013 included, while at the same time becoming less reliable due to the anomalously low densities associated with the very low solar and

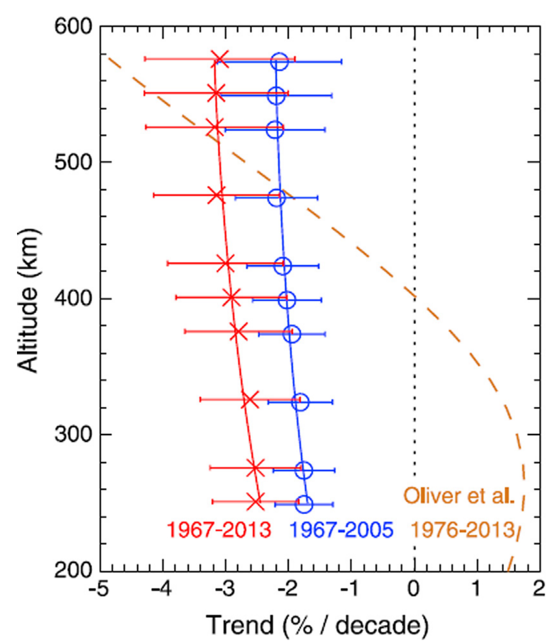

Fig. 7. Thermosphere density trend obtained from orbital drag data for 1967–2005 (blue circles) and 1967–2013 (red crossed) with error bars indicating the 1σ uncertainties. Solid blue and red lines represent fits to NRLMSISE-00, perturbed in such a way as to match the observed density trend profiles. Also shown is the mass density perturbation profile implied by the temperature and composition trends inferred by Oliver et al. (2014) from ground-based incoherent scatter data (dashed orange line), discussed further in Section 5.2. From Emmert (2015). (For interpretation of the references to colour in this figure legend, the reader is referred to the web version of this article.)

geomagnetic activity levels during the 2008/2009 solar minimum period (see Fig. 7). Emmert (2015) and Weng et al. (2020) showed that the reference model used by Emmert (2015) to account for the effects of seasonal, solar activity, and geomagnetic activity variations did not perform well during this period. This is understandable, as that reference model was developed based on data that did not include this unusual solar minimum period. Weng et al. (2020) developed instead an artificial neural network model, based on data including this period. Their model captured the natural variability in the data better, almost regardless of the solar activity proxy that was used. Their results were not significantly dependent on the period of analysis, with trend estimates of −1.6 %/decade and −1.7 %/decade at 400 km altitude for 1967–2005 and 1967–2013, respectively. These trends are slightly smaller than the trend estimated by Emmert (2015) for 1967–2005, but the differences are within the level of uncertainty.

We conclude that an overall global mean thermosphere density trend of at least −1.5 to −2.0 %/decade, slightly increasing with increasing height, is a realistic and reliable result. Modelling studies indicate that this can easily be explained by the increase in CO_2 concentration, with most actually simulating somewhat larger density trends (Qian et al., 2013; Qian et al., 2014; Solomon et al., 2015; Solomon et al., 2018; Solomon et al., 2019; Cnossen, 2020; McInerney et al., 2024). The latest study by McInerney et al. (2024) reported a global mean density trend at 400 km altitude of −5%/decade for the 1970s-2000s period. However, this was for perpetual solar minimum conditions. With realistically varying solar activity, Cnossen (2020) found a smaller average trend of -2.4 ± 0.3%/decade. Solomon et al. (2018) and Solomon et al. (2019) clearly showed the dependence of simulated density trends on solar activity, finding a trend of −1.8%/decade for solar maximum and −2.8%/decade for solar minimum conditions. The solar cycle dependence of observed trends is less clear. Accurate estimation and attribution of trends during solar minimum, using either parametric or neural network reference models, is further complicated by the three major geophysical drivers (solar flux, geomagnetic activity, and CO_2 concentration) all trending toward a cooler thermosphere over the solar minima covered by the orbit-derived density data (Emmert, 2015), which makes it hard to disentangle the effects of these different processes. Analysis of additional orbit-derived data since 2013 could provide better understanding, particularly since the 2019/2020 solar minimum was more typical in terms of the solar and geomagnetic forcing.

Emmert (2015) argued that the observed vertical density trend profile is consistent with an exospheric temperature trend of about −1 to −2 K/decade. Akmaev (2012) calculated an upper limit of −4 to −6 K/decade between 200 and 400 km altitude, based on the reported density trends in this layer. An independent estimate based on the long-term descent of reflection heights of radiowaves in the mesosphere (Bremer and Berger, 2002) and the global mean trend in F_2 peak height (see Section 6.2) provided a similar upper limit (Akmaev, 2012).

5.2. Ion temperature

At low to mid-latitudes, the ion temperature up to about 300–400 km is close to the neutral temperature. Long-term data records of incoherent scatter radar (ISR)-based ion temperature measurements have therefore been used widely to infer thermosphere temperature trends. Even at high latitudes, where the ion temperature tends to be higher than the neutral temperature, especially during disturbed conditions, the long-term change in ion temperature should still provide a useful indication of the neutral temperature trend.

Holt and Zhang (2008) were the first to report a long-term ion temperature trend over Millstone Hill (46.2°N, 288.5°E) based on noon-time ISR data from 1978 to 2007. They found a very large trend of -47 ± 11 K/decade at 375 km altitude. Daytime ion temperature measurements made at other ISR sites, including Saint Santin (44.6°N, 2.2°E), Tromsø (69.6°N, 19.2°E), Sondrestrom (67.0°N, 309.1°E), Chatanika/Poker Flat (65.1°N, 212.6°E), and Arecibo (18.3°N, 66.8°W) have shown similarly large long-term cooling trends of up to several 10s of K/decade (Donaldson et al., 2010; Ogawa et al., 2014; Zhang et al., 2016; Selvaraj et al., 2023). Cooling trends at most of these stations increased with altitude from about 150–200 km up to at least ~300-400 km altitude, while in most cases warming trends were found below 150 km altitude, consistent with the effects of thermal contraction. Donaldson et al. (2010) estimated the thermal subsidence over Saint Santin to range from about 5 km/decade in the lower thermosphere up to about 25 km/decade at 450–500 km altitude. At night time, ion temperature trends are typically (much) smaller (Donaldson et al., 2010; Zhang and Holt, 2013; Zhang et al., 2016; Selvaraj et al., 2023). Zhang and Holt (2013) consequently found a considerably weaker average trend of about −4 K/decade at 200–350 km altitude based on Millstone Hill data from all local times. However, this is still much larger than the thermosphere temperature trend estimated from the globally averaged long-term thermosphere density trend (Emmert, 2015).

It is not clear yet how these different strands of evidence can be reconciled. One point to bear in mind is that local trends in ion temperature are not necessarily representative of the global mean picture. For instance, geomagnetic field changes can induce strong spatial variations in trends. Still, Zhang and Holt (2013) indicated that < 10% of the ion temperature trend at Millstone Hill can be explained by changes in the main magnetic field. Oliver et al. (2013, 2014) suggested that a strongly positive trend in atomic oxygen in the lower thermosphere, around ~120 km altitude, could counteract the thermal contraction associated with thermosphere cooling, resulting in only a small density trend around 400 km altitude, despite a large negative temperature trend at that altitude. However, Emmert (2015) showed that the atomic oxygen and temperature trends inferred by Oliver et al. (2014) lead to a density trend profile that is inconsistent with the orbital drag-based results (see Fig. 7). Model simulations indicate that the increase in CO_2 concentration leads to trends in thermosphere mass density that are largely consistent with orbital drag-based density trend estimates (e.g., Qian et al., 2013; Cnossen, 2020).

6. Ionosphere

6.1. D, E, and F_1 layers

Laštovička and Bremer (2004) reviewed observational evidence on long-term trends in the ionosphere below 120 km altitude, coming from rocket-based measurements, riometer data, ionosonde data, and radio wave absorption and reflection height measurements. They found that most data records indicate that the electron density in the *D* and *E* layers of the ionosphere is increasing, while their height is decreasing. Only rocket-based measurements indicated a negative trend in electron density at 90–120 km altitude. However, a more recent study by Friedrich et al. (2017), also based on rocket measurements, suggested there is no significant trend at 95–120 km altitude, while positive trends in electron density were confirmed below (between ~70 and 80–90 km), as well as above 120–130 km altitude.

Bremer (2008) offered the most comprehensive study of long-term trends in the *E* and F_1 layers, analysing data from a network of 71 ionosondes, where other studies used single stations or a smaller selection of stations (e.g., Givishvili et al., 1995; Bremer, 1998; Mikhailov and de la Morena, 2003; Hall et al., 2011; Mikhailov et al., 2017; Danilov and Konstantinova, 2019). His results for the *E* layer are summarized in Fig. 8. Bremer (2008) showed considerable variations in trend magnitude between stations, but found that, on average, the peak electron densities of both the *E* and F_1 layers had increased, as indicated by average positive trends in the critical frequencies f_oE and f_oF_1 of $+0.013 \pm 0.005$ MHz/decade and $+0.019 \pm 0.011$ MHz/decade, respectively. The *E* layer height, $h'E$, showed a global average long-term trend of -0.29 ± 0.20 km/decade. Bremer (2008) suggested that there might be a small systematic dependence of these trends on latitude and longitude, but the statistical significance of these dependencies was low (see also Elias et al. (2022)). Danilov and Konstantinova (2019) also suggested trends in f_oE depend on latitude, but based on an analysis of only 5 stations, so this at most provides very limited evidence. Others have argued that trends in f_oE can be fully explained by long-term variations in solar activity and become non-significant when these effects are properly taken into account (Mikhailov et al., 2017), although this view is not generally accepted.

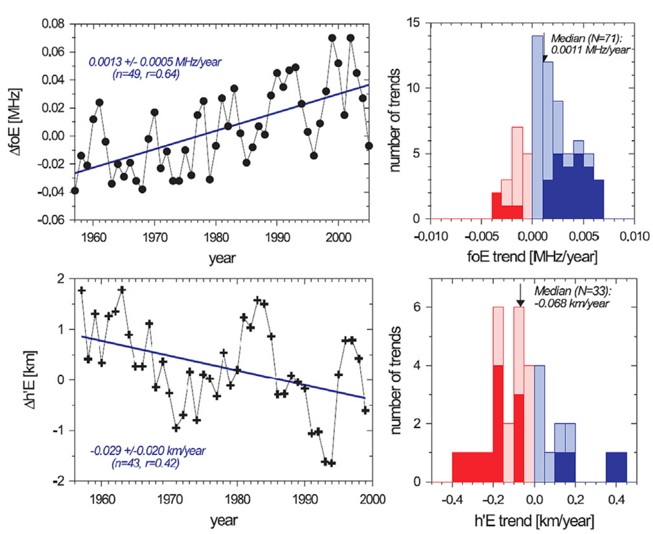

Fig. 8. Top: global mean trend in f_oE based on observations at 71 ionosonde stations (left) and a histogram of the individual trends (right). Bottom: same but for $h'E$, based on observations at 33 ionosonde stations. From Bremer (2008).

6.2. F_2 peak

Bremer (1992) was the first to report a significant lowering of the annual mean height of the peak of the ionospheric F_2 layer, h_mF_2, over Juliusruh (54.6°N, 13.4°E), finding a trend of −2.4 km/decade between 1957 and 1990. Many studies have followed since, but reported trend magnitudes vary enormously with location, season, and local time – sometimes even in sign (e.g., Marin et al., 2001; Bremer et al., 2004; Danilov, 2006). Long-term trends in the critical frequency of the F_2 layer, f_oF_2, are generally found to be weak and not necessarily significantly different from zero (Laštovička et al., 2006; Bremer et al., 2012; Mielich and Bremer, 2013; Laštovička, 2022), although f_oF_2 trend magnitudes do also vary with location, season and local time (e.g. Elias and de Adler, 2006a; Elias and de Adler, 2006b; Danilov, 2015). Some studies have suggested a systematic dependence of trends in h_mF_2 and/or f_oF_2 on latitude (Danilov and Mikhailov, 1999), longitude (Bremer, 1998; Marin et al., 2001; Jarvis, 2009) or proximity to seashores (Bencze, 2007; Bencze, 2009), but other studies found no particular geographic patterns (Upadhyay and Mahajan, 1998; Danilov, 2003; Bremer et al., 2004; Cnossen and Franzke, 2014). Given the lack of uniformity in spatial data coverage, together with differences in temporal data coverage between stations, it does not seem feasible to establish a reliable global picture of spatial variations in trends in h_mF_2 or f_oF_2 to rule any of these possibilities firmly in or out.

This is unfortunate, as a global picture would have been helpful in distinguishing between different drivers that could be responsible for long-term trends in F_2 layer parameters. Based on theoretical work and modelling studies, the increase in CO_2 concentration should have at most a minor effect on f_oF_2 (Rishbeth, 1990; Rishbeth and Roble, 1992; Mikhailov, 2006; Cnossen, 2014) and a spatially relatively uniform effect on h_mF_2 (Cnossen, 2014;

Qian et al., 2021). In contrast, main magnetic field changes can cause large trends with strong spatial structure in both f_oF_2 and h_mF_2, but primarily over South America and the southern part of the Atlantic Ocean, with much smaller (even negligible) effects in most other parts of the world (Cnossen, 2014; Qian et al., 2021).

As main magnetic field effects tend to cancel out in a global average (e.g., Qian et al., 2021), an average of the trends in h_mF_2 and f_oF_2 obtained from the data of many stations can provide some indication of the CO_2-induced trend in these parameters, as long as other possible drivers, in particular solar and geomagnetic activity variations, have been appropriately accounted for. Mielich and Bremer (2013) reported a global mean trend in f_oF_2 for 1948–2006 that was negative but small and not significantly different from zero, based on an analysis of data from 124 stations. Their mean trend in h_mF_2 for 1948–2006, based on data from 113 stations, was -0.96 ± 0.39 km/decade. This is in good agreement with global mean CO_2-induced trends estimated from model simulations (Solomon et al., 2018; Solomon et al., 2019).

6.3. Topside ionosphere

Holt and Zhang (2008) and Zhang et al. (2011) examined the electron density trends in the topside ionosphere, above the F_2 peak, at Millstone Hill (46.2°N, 288.5°E), based on ISR data. Using data from 1978 to 2007, Holt and Zhang (2008) found a negative trend in electron density at 375 km, but this was not statistically significant. Zhang et al. (2011) expanded the dataset to 1968–2006 and did find a significant negative trend at 375 km altitude, of about -0.3 %/decade. At higher altitudes, the trend magnitude decreased, until it was no longer significant at 525 km altitude. They further noted that electron density trends in the upper F region for the 1995–2006 period were nearly double those for the 1968–2006 period.

Cai et al. (2019) put together a large volume of topside electron density data from a series of satellites from the Defense Meteorological Satellite Program (DMSP), using measurements made at 60°S-60°N between 1995 to 2017, at an average altitude of 860 km. They analyzed the data both with standard linear regression and with an artificial neuron network (ANN), but as the latter method appeared to capture seasonal variations in the data better, this was used subsequently for trend analysis. They focused on the electron density trend for 18 magnetic local time (MLT), which was found to vary considerably with latitude, longitude and season, ranging from ~ -2 to $\sim +2$ %/decade. Based on simulations with the Thermosphere-Ionosphere-Electrodynamics General Circulation Model (TIE-GCM), Cai et al. (2019) argued that the long-term variation in the geomagnetic field is the dominant driver of these trends and their spatial structure, while the increase in CO_2 concentration plays a smaller role.

6.4. Total electron content (TEC)

Global Positioning Satellite (GPS) data have been used to examine long-term trends in TEC. While a first study by Lean et al. (2011) indicated a positive global mean trend in TEC, later studies by Lean et al. (2016) and Laštovička et al. (2017) contested this finding and identified at most a weak negative trend. Both concluded that data records are still too short (at most ~20 years) to detect a reliable long-term trend in global mean TEC, and it may be that there is no significant global mean long-term trend. Nonetheless, Emmert et al. (2017) found that there was a change in global mean TEC of -9.3% between the solar minima of 1996 and 2008 that could not be attributed to differences in the F10.7 and Kp indices of solar and geomagnetic activity.

The spatial structure in TEC trends found by Lean et al. (2016) is quite interesting: they showed this consists of bands of both positive and negative trends aligned with the magnetic equator, with local trends being as much as an order of magnitude larger than the global average trend. This kind of dependence on magnetic latitude is in good agreement with a more recent analysis by Andima et al. (2019) of the TEC trends over the African low-latitude region. They found largely negative trends, which were strongest near the magnetic equator, and less negative, or even positive, around the crests of the equatorial ionization anomaly (EIA). The dependence on magnetic latitude suggests that changes in the main magnetic field likely play a role in driving these trends in TEC. Modelling work has indeed confirmed that main magnetic field changes can cause significant changes in TEC, with a similar dependency on magnetic latitude as indicated by observations (Cnossen and Maute, 2020).

7. Forward look

7.1. Trend prediction

The increase in CO_2 concentration is likely to be the most important driver of global mean trends in the middle and upper atmosphere. Early studies often adopted "doubled CO_2" scenarios to provide an indication of future changes (e.g., Roble and Dickinson, 1989; Akmaev and Fomichev, 1998; Qian et al., 2009). However, to plan properly for, for instance, future thermosphere density reductions, more detailed information will be necessary.

One option is to follow the approach taken in the Coupled Model Intercomparison Project (CMIP), which feeds into the Intergovernmental Panel on Climate Change (IPCC) Assessment Reports. Each CMIP phase has defined a range of future scenarios, initially called Representative Concentration Pathways (RCPs) (Meinshausen et al., 2011; van Vuuren et al., 2011) and more recently updated to Shared Socio-economic Pathways (SSPs) (O'Neill et al., 2016). These scenarios are widely used for climate change projections in the lower atmosphere and can in principle be used at higher altitudes as well, but with some caveats. First, the RCP and SSP scenarios do not include main magnetic field changes. For the neutral part of the upper atmosphere, this is at most a minor problem, but for the ionosphere it is important to consider how the magnetic field is changing too. Second, the solar forcing that may be used in conjunction with an RCP or SSP becomes increasingly dominant at higher altitudes. The solar forcing for CMIP6 included for the first time both radiative and particle forcing (Matthes et al., 2017), which are both important for the upper atmosphere. But as neither can be predicted well, not even just one cycle ahead, the future forcing must rely again on scenarios. Matthes et al. (2017) defined both a reference scenario, which consisted of a plausible level of solar activity and variability on all timescales, including centennial, and an extreme scenario with an exceptionally low level of solar activity. This may be adequate for climate change projections in the lower atmosphere, but given the much greater sensitivity of the upper atmosphere to solar activity, a wider range of plausible scenarios, especially in terms of long-term solar variability, may be needed to explore the uncertainties in climate projections at higher altitudes.

Cnossen (2022) recently provided a projection of the climate in the thermosphere and ionosphere following SSP 2–4.5, a moderate scenario, using a simulation with the WACCM-X 2.0. This simulation also included a prediction of main magnetic field changes by Aubert (2015) and used the reference scenario for solar radiative and particle forcing by Matthes et al. (2017). Global mean thermosphere density trends for 2015–2070 were shown to be about twice as large as for the period 1950–2015, as expected for a more rapid increase in CO_2 concentration. Climate change in the ionosphere was also stronger for 2015–2070 than for 1950–2015, but varied strongly with location, with the largest changes expected in the region of ~50°S–20°N and ~90°–0°W. These were mainly associated with large predicted magnetic field changes in this region.

Brown et al. (2021) investigated a broader range of future emission scenarios, but at a fixed, low solar activity level, by conducting a series of simulations with WACCM-X with different CO_2 concentrations and mapping these onto four different RCPs, ranging from "best case" (RCP2.6) to "worst case" (RCP8.5). Their results focused on the thermosphere density response to CO_2, as this has important implications for space debris and long-term satellite mission planning. They showed that even under the "best case" scenario, thermosphere density is expected to decrease by ~30% by 2050 relative to the year 2000, which would also increase orbital lifetimes by about 30%. Under the worst case scenario, the same reduction in density would already be reached by 2030 according to their results. However, we note that the historical trend for 1975–2005 at 400 km altitude (−5.8%/decade) found by Brown et al. (2021) is on the large side compared to other modelling results and observations (see Section 5.1). This suggests that their projected density trends could also be relatively large. Brown et al. (2024) expanded on the results of Brown et al. (2021) by conducting a similar set of simulations for a fixed high solar activity level, as well as a few additional simulations at fixed CO_2 levels, but with varying solar activity levels. This enabled them to define scaling factors which describe the combined dependence of thermosphere density on solar radiative activity and CO_2 concentration. These scaling factors can then be applied to the outputs of empirical models to account for future CO_2-induced thermospheric density reductions, to facilitate inclusion of long-term trends in applications such as, for example, orbital lifetime estimation and debris environment modelling.

7.2. Incorporation of trends in (semi-) empirical models

Historically, major empirical models of the upper atmosphere and ionosphere have been "static climatologies", where a climatology is defined as a description of the average observed behavior of an environmental system as a function of location, relevant cyclical temporal variables (e.g., day of year, local time), and external physical drivers (e.g., solar activity). A climatology is static if it does not contain explicit time dependence such as a linear trend term, although it may implicitly depend on time via the external drivers. By this definition, the Jacchia-Bowman (Bowman et al., 2008), DTM (Bruinsma and Boniface, 2021), and MSIS (Emmert et al., 2022) series of neutral temperature and density models, as well as the Horizontal Wind Model (HWM) (Drob et al., 2015) and IRI (Bilitza et al., 2022), are all static climatologies. On the other hand, the International Geomagnetic Reference Field (IGRF) (Alken et al., 2021) can be viewed as a time-dependent climatology, since a set of new parameter values is added to the model every five years, including linear trend terms that allow the model to be extrapolated into the future.

An important application of static climatologies is their use as a reference for detecting and quantifying long-term trends in observations (e.g., Emmert et al., 2008). By subtracting the climatological predictions, known (i.e., observationally well characterized) variations are largely filtered from the data, and the remaining anomalies can be statistically analyzed for trends. However, as we gain quantitative and physical understanding of such trends, it makes sense to incorporate them into empirical models. This could be done by incorporating explicit trend terms into a model or updating the model parameter values periodically (as is done for IGRF). With this approach, however, the ability to project the model into the past or future is limited by the extrapolative assumption that the trend terms are static. Alternatively, if the long-term trend can be attributed to specific drivers, then the driver itself can be incorporated as an input argument to an empirical model. Emmert (2015) used this approach in the construction of the specialized empirical model GAMDM2 (global average mass density model), which represents orbital drag-derived mass density data and depends on the deseasonalized tropospheric CO_2 concentration. As discussed earlier, theoretical considerations and physics-based model simulations indicate that CO_2 is a major driver of upper atmospheric trends. Because the atmospheric CO_2 concentration is currently increasing monotonically (and approximately linearly on a timescale of a few decades), incorporation of CO_2 dependence into a model empirically attributes temporal trends largely to this driver.

Fig. 9 shows an example of how incorporation of CO_2 dependence into an empirical model can be used to predict future climatological states of the upper atmosphere. It depicts the projected centennial change in thermospheric mass density RCPs used in the Fifth Assessment Report (AR5) of the IPCC (IPCC, 2014). The density projections are based on the height and CO_2 dependencies of GAMDM2, which covers altitudes from 250 km to 575 km. To extrapolate to higher altitudes (i.e., into the helium-dominated regime of the atmosphere), NRLMSISE-00 (Picone et al., 2002) temperature and density parameters were tuned to match the GAMDM2-predicted change profiles, following the method described by Emmert (2015). For comparison, the mass density change profile simulated by Roble and Dickinson (1989) for CO_2 doubling is also shown and is similar to the GAMDM2 projection for RCP 6.0 (which has a centennial CO_2 change slightly smaller than double). On the other hand, the projections by Brown et al. (2021) indicate considerably stronger density reductions by 2100.

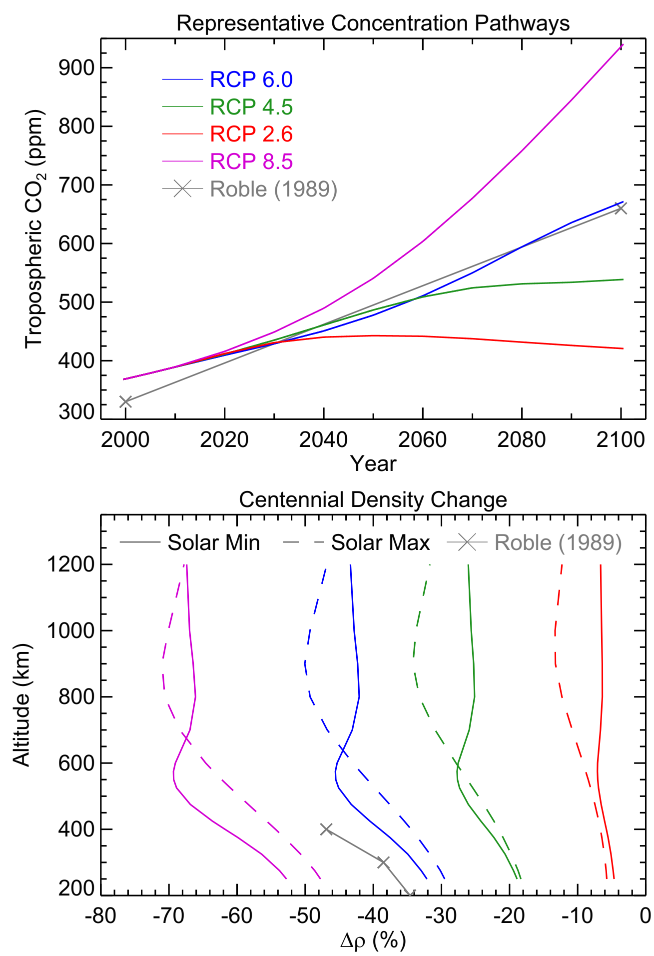

Fig. 9. Top: CO_2 representative concentration pathways (RCPs) (van Vuuren et al., 2011). Also shown (grey) is the CO_2 doubling scenario used in the thermosphere-ionosphere simulations of Roble and Dickinson (1989). Bottom: Projected thermospheric mass density change from 2000 to 2100 for each RCP derived from the GAMDM2 empirical model (Emmert et al., 2014) and extrapolated to higher altitudes by scaling NRLMSISE-00 temperature and density parameters, following Emmert (2015). Results are shown for solar minimum (F10.7 = 70, solid line) and solar maximum (F10.7 = 200, dashed line). Also shown (grey) is the density change profile derived from the Roble and Dickinson (1989) solar minimum, CO_2 doubling simulation.

Motivated by the importance of CO_2 to the radiative balance of the atmosphere, the addition of a CO_2 component to MSIS has been initiated and is currently under development. The modeled CO_2 profile will be scaled to the ground-level concentration, which will be directly specifiable as an input argument or indirectly via the year input argument combined with ground-level measurements and trends. It is envisioned that the MSIS temperature profile will eventually be coupled to the CO_2 component, so that the model's temperature and density will capture the observed long-term atmospheric changes.

Incorporation of long-term trends in ionospheric empirical models, such as IRI, is likely to be more complicated, as the ionosphere is not only affected by the increase in CO_2 concentration, but also by geomagnetic field changes. Effects of geomagnetic field changes are much more difficult to characterize than effects of CO_2 increases, as they vary strongly with location, in addition to local time and seasonal dependencies. Currently, IRI can capture some of the long-term ionospheric trends associated with main magnetic field changes through the use of magnetic coordinates rather than geographic coordinates. However, not all effects of geomagnetic field changes are accounted for in this way (Cnossen and Maute, 2020), as illustrated in Fig. 10. Especially in regions where magnetic field changes have been relatively large, this could lead to significant inaccuracies. Further, IRI makes use of the IG12 index for some of its outputs. This index is directly based on ionosonde data from selected stations and will therefore

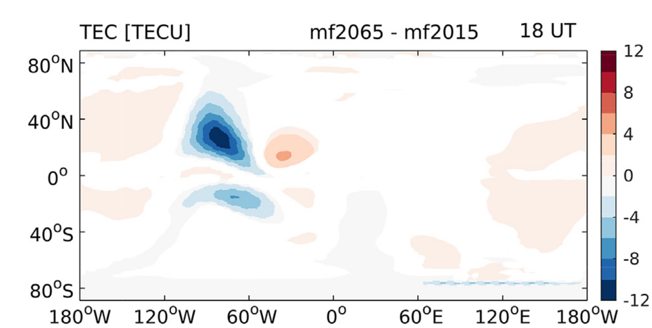

Fig. 10. Predicted change in TEC from 2015 to 2065 at 18 UT, plotted in magnetic latitude and geographic longitude, averaged over all days of the year. From Cnossen and Maute (2020).

have a long-term trend embedded in it. However, whether this is a reasonable global representation has not been verified. One of the stations used for IG12 is Port Stanley (52°S, 58°W, which could be considerably affected by local geomagnetic field changes (see, e.g., Cnossen, 2014). Such local effects could then potentially be introduced into the rest of the world through the use of the IG12 index, which is clearly something that should be avoided. Finding a pathway to include long-term trends in IRI in an appropriate and consistent way will require some careful consideration of these issues.

8. Summary and conclusions

The increase in CO_2 concentration is the main driver of global mean climate change in the mesosphere, thermosphere, and ionosphere. The trend in the CO_2 concentration itself above 90 km altitude initially appeared to be considerably stronger than in the troposphere (Emmert et al., 2012; Yue et al., 2015), but this turned out to be due to data quality and methodology problems (Qian et al., 2017; Rezac et al., 2018). The most recent evidence shows that the CO_2 concentration in the lower thermosphere increases at a rate of 5–7%/decade (Pramitha et al., 2023), which is not significantly different from the tropospheric trend.

Satellite-based observational evidence indicates that the mesosphere has been cooling by up to −1.2 K/decade at low- to mid-latitudes ($\leq 45°$) (Li et al., 2021) during the last 20–30 years. This is in reasonable agreement with model simulations (Akmaev and Fomichev, 1998; Garcia et al., 2019; Ramesh et al., 2020) and can be largely attributed to the increase in CO_2 concentration. Earlier studies, based primarily on rocketsonde and lidar measurements, indicated somewhat larger temperature trends (Beig et al., 2003; Beig, 2011), which could be explained by the additional cooling caused by ozone depletion during the 1980s and early 1990s. At high latitudes (64–70°) during local summer, satellite observations from the last 20–30 years also suggest stronger cooling, up to −2 K/decade, with the associated thermal contraction causing a downward shift of constant pressure surfaces of about −100 to −200 m/decade (Bailey et al., 2021). However, it is not clear whether Bailey et al. (2021) may have overestimated the trend by using monthly means for SABER data rather than the recommended bi-monthly means or whether the cooling at high latitude is truly stronger, perhaps due to changes in circulation. It is not yet possible to establish a clear global picture of long-term trends in dynamics in the mesosphere and lower thermosphere, as observed trends in winds and gravity wave activity are limited and vary strongly with location and season. Local observations of temperature in the mesopause region also show rather inconsistent long-term trends. Satellite records, albeit somewhat short still for long-term trend analysis, suggest that trends vary with location, but indicate a global average mesopause temperature trend of -0.75 ± 0.43 K/decade (Zhao et al., 2020).

Orbital data have indicated a thermosphere density trend that slightly increases with altitude, with a value of −1.5 to −2.0 %/decade at 400 km altitude (e.g., Emmert, 2015; Weng et al., 2020). The reported density trend profiles suggest an exospheric temperature trend of about −1 to −2 K/decade (Emmert, 2015), or at least less than −4 to −6 K/decade (Akmaev, 2012). However, the observed trends in ion temperature, which should be close to the neutral temperature up to ~300 km altitude, are considerably larger, at least during daytime, when ISRs in various locations all indicate trends of several 10s of K/decade. Nighttime trends are much smaller, which can explain some of the large discrepancy between estimates of thermosphere temperature trends based on reported density trends versus ion temperature trends. However, Zhang and Holt (2013) found that the trend averaged over all local times at Millstone Hill is still about −4 K/decade at 200–350 km altitude, i.e., at the top end of what is considered possible based on other constraints.

The electron density in the *D* and *E* layers is increasing, while their height is decreasing (Laštovička and Bremer, 2004), consistent with the effects of thermal contraction. While there is considerable spatial variation, on average the critical frequency of the *E* layer has increased by 0.013 ± 0.005 MHz/decade, while its height has decreased by 0.29 ± 0.20 km/decade (Bremer, 2008). The critical frequency of the F_1 layer has an average trend of $+0.019 \pm 0.011$ MHz/decade. The global mean trend in the critical frequency of the F_2 layer is not significantly different from zero, while the mean trend in its peak height is -0.96 ± 0.39 km/decade (Mielich and Bremer, 2013), in good agreement with the expected effects of the increase in CO_2 concentration (Solomon et al., 2018; Solomon et al., 2019). Trends of the electron density in the topside ionosphere range from ~ -2 to $\sim +2$ %/decade, but here changes in the main magnetic field appear to be the dominant driver (Cai et al., 2019). There also appears to be a weak negative global mean trend in TEC, but data records are still too short to establish this reliably (Lean et al., 2016; Laštovička et al., 2017). Further, there are large spatial variations in TEC trends, which follow main magnetic field features (Lean et al., 2016; Andima et al., 2019). This indicates that main magnetic field changes are also an important driver of long-term change in the ionosphere, especially from the F_2 peak upward.

Long-term trends are for the most part not currently included in (semi-) empirical models of the mesosphere, thermosphere and/or ionosphere, which can be problematic for practical applications that make use of these models. However, work is underway to include a CO_2 term in MSIS. Once this is done, it will be straightforward to explore a range of future scenarios with this model, both in terms of CO_2 concentration and solar activity. This should provide valuable information on the range of outcomes that is possible, depending (partly) on our actions, and the uncertainty in future projections. In the meantime, the scaling factors of Brown et al. (2024) may be used for applications requiring thermosphere density projections. For the ionosphere, especially for the F_2 peak, topside ionosphere, and TEC, changes in the magnetic field need to be accounted for in addition to the increase in CO_2 concentration. Only some of these effects can be captured through the use of magnetic coordinates. Further, in IRI specifically, care must be taken with outputs relying on the IG12 index, which uses local ionosonde data and could therefore have locally induced trends embedded in it. This will need to be addressed if long-term trends are to be represented properly in IRI.

Finally, we take this opportunity to point out that there is a continued need to monitor the climate of the upper atmosphere, both with ground-based and satellite-based measurements, which are complementary. While we have a reasonably clear, quantitative picture of global mean trends in various important parameters of the upper atmosphere, it is essential that predictions are checked against reality. Continued measurements are also required to resolve remaining inconsistencies, reduce uncertainties, and improve our understanding of spatial variations and local time and seasonal dependencies in trends (see also Zhang et al., 2023). It is therefore vital that existing observational facilities that maintain long-term datasets are supported to continue their work. As satellite missions are finite, it is also crucial that follow-on missions are planned sufficiently early on to ensure data continuity, where a period of overlap is essential to allow for calibration. Research in observing trends in critical climate parameters (Loeb et al., 2009) has shown that gaps in satellite data records prohibit accurate assessement of trends, even if the succeeding instrument is an identical copy of its predecessor. We are currently in a precarious situation when it comes to monitoring the mesosphere and lower thermosphere region, as MLS will soon be switched off and SABER is also aging. This must be addressed to keep monitoring and improving our understanding of climate change at all levels in the atmosphere.

Declaration of Competing Interest

The authors declare that they have no known competing financial interests or personal relationships that could have appeared to influence the work reported in this paper.

Acknowledgments

I. Cnossen was supported by a Natural Environment Research Council (NERC) Independent Research Fellowship (NE/R015651/1). J. Emmert acknowledges support from the Office of Naval Research Marine Meteorology and Space Weather Program. S. Zhang was supported by NASA grant 80NSSC21K1315 and NSF award AGS-1952737. I. Cnossen, M. Mlynczak and S. Zhang acknowledge support from the International Space Science Institute (ISSI) in Bern, through ISSI International Team project 544 ”Impacts of climate change on the middle and upper atmosphere and atmospheric drag of space objects”.

References

Akmaev, R., 2012. On estimation and attribution of long-term temperature trends in the thermosphere. J. Geophys. Res.: Space Phys. 117 (A9). https://doi.org/10.1029/2012ja018058.

Akmaev, R.A., Fomichev, V., 1998. Cooling of the mesosphere and lower thermosphere due to doubling of CO_2. Ann. Geophys. 16 (11), 1501–1512. https://doi.org/10.1007/s00585-998-1501-z.

Akmaev, R.A., Fomichev, V.I., Zhu, X., 2006. Impact of middle-atmospheric composition changes on greenhouse cooling in the upper atmosphere. J. Atmos. Solar Terr. Phys. 68 (17), 1879–1889. https://doi.org/10.1016/j.jastp.2006.03.008.

Alken, P., Thébault, E., Beggan, C.D., et al., 2021. International geomagnetic reference field: the thirteenth generation. Earth, Planets and Space 73 (1). https://doi.org/10.1186/s40623-020-01288-x.

Andima, G., Amabayo, E.B., Jurua, E., et al., 2019. Modeling of GPS total electron content over the african low-latitude region using empirical orthogonal functions. Ann. Geophys. 37 (1), 65–76. https://doi.org/10.5194/angeo-37-65-2019.

Aubert, J., 2015. Geomagnetic forecasts driven by thermal wind dynamics in the Earth’s core. Geophys. J. Int. 203 (3), 1738–1751. https://doi.org/10.1093/gji/ggv394.

Bailey, S.M., Thurairajah, B., Hervig, M.E., et al., 2021. Trends in the polar summer mesosphere temperature and pressure altitude from satellite observations. J. Atmos. Solar Terr. Phys. 220, 105650. https://doi.org/10.1016/j.jastp.2021.105650.

Beig, G., 2011. Long-term trends in the temperature of the mesosphere/lower thermosphere region: 1. anthropogenic influences. J. Geophys. Res.: Space Phys. 116 (A2). https://doi.org/10.1029/2011ja016646, n/a–n/a.

Beig, G., Keckhut, P., Lowe, R.P., et al., 2003. Review of mesospheric temperature trends. Rev. Geophys. 41 (4). https://doi.org/10.1029/2002rg000121.

Bencze, P., 2007. What do we know of the long-term change of the Earth’s ionosphere? Adv. Space Res. 40 (7), 1121–1125. https://doi.org/10.1016/j.asr.2007.01.078.

Bencze, P., 2009. Geographical distribution of long-term changes in the height of the maximum electron density of the F region: A nonmigrating-tide effect? J. Geophys. Res.: Space Phys. 114 (A6), A06304. https://doi.org/10.1029/2008ja013492.

Bilitza, D., Pezzopane, M., Truhlik, V., et al., 2022. The International Reference Ionosphere model: A review and description of an ionospheric benchmark. Rev. Geophys. 60 (4). https://doi.org/10.1029/2022rg000792.

Boley, A.C., Byers, M., 2021. Satellite mega-constellations create risks in Low Earth Orbit, the atmosphere and on Earth. Scient. Rep. 11 (1). https://doi.org/10.1038/s41598-021-89909-7.

Bowman, B., Tobiska, W.K., Marcos, F., et al., 2008. A new empirical thermospheric density model JB2008 using new solar and geomagnetic indices. In: AIAA/AAS Astrodynamics Specialist Conference and Exhibit. American Institute of Aeronautics and Astronautics. https://doi.org/10.2514/6.2008-6438.

Bremer, J., 1992. Ionospheric trends in mid-latitudes as a possible indicator of the atmospheric greenhouse effect. J. Atmos. Terr. Phys. 54 (11–12), 1505–1511. https://doi.org/10.1016/0021-9169(92)90157-g.

Bremer, J., 1998. Trends in the ionospheric E and F regions over Europe. Ann. Geophys. 16 (8), 986–996. https://doi.org/10.1007/s00585-998-0986-9.

Bremer, J., 2008. Long-term trends in the ionospheric E and F1 regions. Ann. Geophys. 26 (5), 1189–1197. https://doi.org/10.5194/angeo-26-1189-2008.

Bremer, J., Alfonsi, L., Bencze, P., et al., 2004. Long-term trends in the ionosphere and upper atmosphere parameters. Annals of geophysics 47 (2–3), 1009–1029.

Bremer, J., Berger, U., 2002. Mesospheric temperature trends derived from ground-based lf phase-height observations at mid-latitudes: comparison with model simulations. J. Atmos. Solar Terr. Phys. 64 (7), 805–816. https://doi.org/10.1016/s1364-6826(02)00073-1.

Bremer, J., Damboldt, T., Mielich, J., et al., 2012. Comparing long-term trends in the ionospheric F2-region with two different methods. J. Atmos. Solar Terr. Phys. 77, 174–185. https://doi.org/10.1016/j.jastp.2011.12.017.

Brown, M., Lewis, H., Kavanagh, A., et al., 2024. accepted). Future climate change in the thermosphere under varying solar activity conditions. J. Geophys. Res.: Space Phys..

Brown, M.K., Lewis, H.G., Kavanagh, A.J., et al., 2021. Future decreases in thermospheric neutral density in Low Earth Orbit due to carbon dioxide emissions. J. Geophys. Res.: Atmos. 126 (8). https://doi.org/10.1029/2021jd034589.

Bruevich, E., Bruevich, V., 2019. Long-term trends in solar activity. variations of solar indices in the last 40 years. Res. Astron. Astrophys. 19 (7), 090. https://doi.org/10.1088/1674-4527/19/7/90.

Bruinsma, S., Boniface, C., 2021. The operational and research DTM-2020 thermosphere models. J. Space Weather Space Clim. 11, 47. https://doi.org/10.1051/swsc/2021032.

Cai, Y., Yue, X., Wang, W., et al., 2019. Long-term trend of topside ionospheric electron density derived from DMSP data during 1995–2017. J. Geophys. Res.: Space Phys. https://doi.org/10.1029/2019ja027522.

Clilverd, M.A., Clark, T.D.G., Clarke, E., et al., 1998. Increased magnetic storm activity from 1868 to 1995. J. Atmos. Solar Terr. Phys. 60 (10), 1047–1056. https://doi.org/10.1016/s1364-6826(98)00049-2.

Clilverd, M.A., Clarke, E., Ulich, T., et al., 2005. Reconstructing the long-term aa index. J. Geophys. Res. 110 (A7). https://doi.org/10.1029/2004ja010762.

Clilverd, M.A., Ulich, T., Jarvis, M.J., 2003. Residual solar cycle influence on trends in ionospheric F2-layer peak height. J. Geophys. Res. 108 (A12). https://doi.org/10.1029/2003ja009838.

Cnossen, I. (2012). Greenhouse gases – emission, measurement and management. chapter Climate change in the upper atmosphere. (pp. 315–336). InTech. doi:10.5772/32565.

Cnossen, I., 2014. The importance of geomagnetic field changes versus rising CO_2 levels for long-term change in the upper atmosphere. J. Space Weather Space Clim. 4, A18. https://doi.org/10.1051/swsc/2014016.

Cnossen, I., 2020. Analysis and attribution of climate change in the upper atmosphere from 1950 to 2015 simulated by WACCM-X. J. Geophys. Res.: Space Phys. 125 (12). https://doi.org/10.1029/2020ja028623.

Cnossen, I., 2022. A realistic projection of climate change in the upper atmosphere into the 21st century. Geophys. Res. Lett. 49 (19). https://doi.org/10.1029/2022gl100693.

Cnossen, I., Franzke, C., 2014. The role of the sun in long-term change in the F2 peak ionosphere: New insights from EEMD and numerical modeling. J. Geophys. Res.: Space Phys. 119 (10), 8610–8623. https://doi.org/10.1002/2014ja020048.

Cnossen, I., Liu, H., Lu, H., 2016. The whole atmosphere response to changes in the Earth's magnetic field from 1900 to 2000: An example of "top-down" vertical coupling. J. Geophys. Res.: Atmos. 121 (13), 7781–7800. https://doi.org/10.1002/2016jd024890.

Cnossen, I., Matzka, J., 2016. Changes in solar quiet magnetic variations since the Maunder Minimum: A comparison of historical observations and model simulations. J. Geophys. Res.: Space Phys. 121 (10), 10520–10535. https://doi.org/10.1002/2016ja023211.

Cnossen, I., Maute, A., 2020. Simulated trends in ionosphere-thermosphere climate due to predicted main magnetic field changes from 2015 to 2065. J. Geophys. Res.: Space Phys. 125 (3). https://doi.org/10.1029/2019ja027738.

Cnossen, I., Richmond, A.D., 2008. Modelling the effects of changes in the Earth's magnetic field from 1957 to 1997 on the ionospheric hmF2 and foF2 parameters. J. Atmos. Solar Terr. Phys. 70 (11–12), 1512–1524. https://doi.org/10.1016/j.jastp.2008.05.003.

Cnossen, I., Richmond, A.D., 2013. Changes in the Earth's magnetic field over the past century: Effects on the ionosphere-thermosphere system and solar quiet (sq) magnetic variation. J. Geophys. Res.: Space Phys. 118 (2), 849–858. https://doi.org/10.1029/2012ja018447.

Danilov, A., 2006. Progress in studies of the trends in the ionosphere F region. Phys. Chem. Earth, Parts A/B/C 31 (1–3), 34–40. https://doi.org/10.1016/j.pce.2005.02.002.

Danilov, A., 2015. Seasonal and diurnal variations in f_of_2 trends. J. Geophys. Res.: Space Phys. 120 (5), 3868–3882. https://doi.org/10.1002/2014ja020971.

Danilov, A., Konstantinova, A., 2019. Diurnal and seasonal variations in long-term changes in the E-layer critical frequency. Adv. Space Res. 63 (1), 359–370. https://doi.org/10.1016/j.asr.2018.10.015.

Danilov, A., Konstantinova, A., 2020. Trends in foF2 and the 24th solar activity cycle. Adv. Space Res. 65 (3), 959–965. https://doi.org/10.1016/j.asr.2019.10.038.

Danilov, A.D., 2003. Long-term trends of foF2 independent of geomagnetic activity. Ann. Geophys. 21 (5), 1167–1176. https://doi.org/10.5194/angeo-21-1167-2003.

Danilov, A.D., Berbeneva, N.A., 2021. Some applied aspects of the study of trends in the upper and middle atmosphere. Geomag. Aeron. 61 (4), 578–588. https://doi.org/10.1134/s0016793221040046.

Danilov, A.D., Konstantinova, A.V., 2016. Trends in the critical frequency foF2 after 2009. Geomag. Aeron. 56 (3), 302–310. https://doi.org/10.1134/s0016793216030026.

Danilov, A.D., Mikhailov, A.V., 1999. Spatial and seasonal variations of the F2 long-term trends. Ann. Geophys. 17 (9), 1239–1243. https://doi.org/10.1007/s00585-999-1239-2.

Das, U., 2021. Spatial variability in long-term temperature trends in the middle atmosphere from SABER/TIMED observations. Adv. Space Res. 68 (7), 2890–2903. https://doi.org/10.1016/j.asr.2021.05.014.

Dawkins, E.C.M., Stober, G., Janches, D., et al., 2023. Solar cycle and long-term trends in the observed peak of the meteor altitude distributions by meteor radars. Geophys. Res. Lett. 50 (2). https://doi.org/10.1029/2022gl101953.

Donaldson, J.K., Wellman, T.J., Oliver, W.L., 2010. Long-term change in thermospheric temperature above Saint Santin. J. Geophys. Res.: Space Phys. 115 (A11). https://doi.org/10.1029/2010ja015346.

Drob, D.P., Emmert, J.T., Meriwether, J.W., et al., 2015. An update to the horizontal wind model (HWM): The quiet time thermosphere. Earth and Space Science 2 (7), 301–319. https://doi.org/10.1002/2014ea000089.

Elias, A.G., 2009. Trends in the F2 ionospheric layer due to long-term variations in the Earth's magnetic field. J. Atmos. Solar Terr. Phys. 71 (14–15), 1602–1609. https://doi.org/10.1016/j.jastp.2009.05.014.

Elias, A.G., 2014. Filtering ionosphere parameters to detect trends linked to anthropogenic effects. Earth, Planets and Space 66 (1), 113. https://doi.org/10.1186/1880-5981-66-113.

Elias, A.G., de Adler, N.O., 2006a. Earth magnetic field and geomagnetic activity effects on long-term trends in the F2 layer at mid-high latitudes. J. Atmos. Solar Terr. Phys. 68 (17), 1871–1878. https://doi.org/10.1016/j.jastp.2006.02.008.

Elias, A.G., de Adler, N.O., 2006b. foF2 long-term trends at the southern crest of the equatorial anomaly. Phys. Chem. Earth, Parts A/B/C 31 (1–3), 63–67. https://doi.org/10.1016/j.pce.2005.02.004.

Elias, A.G., de Haro Barbas, B.F., Shibasaki, K., et al., 2014. Effect of solar cycle 23 in foF2 trend estimation. Earth, Planets and Space 66 (1). https://doi.org/10.1186/1880-5981-66-111.

Elias, A.G., de Haro Barbas, B.F., Zossi, B.S., et al., 2022. Review of long-term trends in the equatorial ionosphere due the geomagnetic field secular variations and its relevance to space weather. Atmosphere 13 (1), 40. https://doi.org/10.3390/atmos13010040.

Emmert, J.T., 2015. Altitude and solar activity dependence of 1967–2005 thermospheric density trends derived from orbital drag. J. Geophys. Res.: Space Phys. 120 (4), 2940–2950. https://doi.org/10.1002/2015ja021047.

Emmert, J.T., Drob, D.P., Picone, J.M., et al., 2020. NRLMSIS 2.0: A whole-atmosphere empirical model of temperature and neutral species densities. Earth Space Sci. 8 (3). https://doi.org/10.1029/2020ea001321.

Emmert, J.T., Jones, M., Siskind, D.E., et al., 2022. NRLMSIS 2.1: An empirical model of nitric oxide incorporated into MSIS. J. Geophys. Res.: Space Phys. 127 (10). https://doi.org/10.1029/2022ja030896.

Emmert, J.T., Mannucci, A.J., McDonald, S.E., et al., 2017. Attribution of interminimum changes in global and hemispheric total electron content. J. Geophys. Res.: Space Phys. 122 (2), 2424–2439. https://doi.org/10.1002/2016ja023680.

Emmert, J.T., McDonald, S.E., Drob, D.P., et al., 2014. Attribution of interminima changes in the global thermosphere and ionosphere. J. Geophys. Res.: Space Phys. 119 (8), 6657–6688. https://doi.org/10.1002/2013ja019484.

Emmert, J.T., Picone, J.M., Lean, J.L., et al., 2004. Global change in the thermosphere: Compelling evidence of a secular decrease in density. J. Geophys. Res.: Space Phys. 109 (A2). https://doi.org/10.1029/2003ja010176.

Emmert, J.T., Picone, J.M., & Meier, R.R. (2008). Thermospheric global average density trends, 1967–2007, derived from orbits of 5000 near-Earth objects. Geophysical Research Letters, 35(5). doi:10.1029/2007gl032809.

Emmert, J.T., Stevens, M.H., Bernath, P.F., et al., 2012. Observations of increasing carbon dioxide concentration in Earth's thermosphere. Nat. Geosci. 5 (12), 868–871. https://doi.org/10.1038/ngeo1626.

Finlay, C.C., Maus, S., Beggan, C.D., et al., 2010. International Geomagnetic Reference Field: the eleventh generation. Geophys. J. Int. 183 (3), 1216–1230. https://doi.org/10.1111/j.1365-246x.2010.04804.x.

French, W.J.R., Mulligan, F.J., Klekociuk, A.R., 2020. Analysis of 24 years of mesopause region OH rotational temperature observations at davis, antarctica – part 1: long-term trends. Atmos. Chem. Phys. 20 (11), 6379–6394. https://doi.org/10.5194/acp-20-6379-2020.

Friedrich, M., Pock, C., Torkar, K., 2017. Long-term trends in the *D* - and *E* -region based on rocket-borne measurements. J. Atmos. Solar Terr. Phys. 163, 78–84. https://doi.org/10.1016/j.jastp.2017.04.009.

Garcia, R.R., López-Puertas, M., Funke, B., et al., 2016. On the secular trend of CO_x and CO_2 in the lower thermosphere. J. Geophys. Res.: Atmos. 121 (7), 3634–3644. https://doi.org/10.1002/2015jd024553.

Garcia, R.R., Marsh, D.R., Kinnison, D.E. et al., 2007. Simulation of secular trends in the middle atmosphere, 1950–2003. J. Geophys. Res., 112(D9). doi:10.1029/2006jd007485.

Garcia, R.R., Yue, J., Russell, J.M., 2019. Middle atmosphere temperature trends in the twentieth and twenty-first centuries simulated with the whole atmosphere community climate model (WACCM). J. Geophys. Res.: Space Phys. 124 (10), 7984–7993. https://doi.org/10.1029/2019ja026909.

Givishvili, G., Leschenko, L., Shmeleva, O., et al., 1995. Climatic trends of the mid-latitude upper atmosphere and ionosphere. J. Atmos. Terr. Phys. 57 (8), 871–874. https://doi.org/10.1016/0021-9169(94)00084-2.

Gnabahou, D.A., Elias, A.G., Ouattara, F., 2013. Long-term trend of f_oF_2 at a West African equatorial station linked to greenhouse gas increase and dip equator secular displacement. J. Geophys. Res.: Space Phys. 118 (6), 3909–3913. https://doi.org/10.1002/jgra.50381.

Gromenko, O., Kokoszka, P., Zhu, L., et al., 2012. Estimation and testing for spatially indexed curves with application to ionospheric and magnetic field trends. The Annals of Applied Statistics 6 (2). https://doi.org/10.1214/11-aoas524.

Hall, C.M., Rypdal, K., Rypdal, M., 2011. The *E* region at 69°N, 19°E: Trends, significances, and detectability. J. Geophys. Res.: Space Phys. 116 (A5). https://doi.org/10.1029/2011ja016431.

de Haro Barbas, B.F., Elias, A.G., 2015. On the inclusion of data from solar cycle 19 to estimate F2 layer characteristic long term trends. Annals of Geophysics 58 (4). https://doi.org/10.4401/ag-6676.

de Haro Barbas, B.F., Elias, A.G., Cnossen, I., et al., 2013. Long-term changes in solar quiet (Sq) geomagnetic variations related to Earth's magnetic field secular variation. J. Geophys. Res.: Space Phys. 118 (6), 3712–3718. https://doi.org/10.1002/jgra.50352.

de Haro Barbás, B.F., Elias, A.G., Venchiarutti, J.V., et al., 2021. MgII as a solar proxy to filter F2-region ionospheric parameters. Pure Appl. Geophys. 178 (11), 4605–4618. https://doi.org/10.1007/s00024-021-02884-y.

Harris, N.R.P., Hassler, B., Tummon, F., et al., 2015. Past changes in the vertical distribution of ozone – part 3: Analysis and interpretation of trends. Atmos. Chem. Phys. 15 (17), 9965–9982. https://doi.org/10.5194/acp-15-9965-2015.

Hoffmann, P., Rapp, M., Singer, W., et al., 2011. Trends of mesospheric gravity waves at northern middle latitudes during summer. J. Geophys. Res. 116. https://doi.org/10.1029/2011jd015717.

Holt, J.M., Zhang, S.R., 2008. Long-term temperature trends in the ionosphere above Millstone Hill. Geophys. Res. Lett. 35 (5). https://doi.org/10.1029/2007gl031148.

IPCC (2014). Climate Change 2013 – The Physical Science Basis: Working Group I Contribution to the Fifth Assessment Report of the Intergovernmental Panel on Climate Change. Cambridge University Press. doi:10.1017/cbo9781107415324.

Jacobi, C., 2014. Long-term trends and decadal variability of upper mesosphere/lower thermosphere gravity waves at midlatitudes. J. Atmos. Solar Terr. Phys. 118, 90–95. https://doi.org/10.1016/j.jastp.2013.05.009.

Jacobi, C., Lilienthal, F., Geißler, C., et al., 2015. Long-term variability of mid-latitude mesosphere-lower thermosphere winds over Collm (51°N, 13°E). J. Atmos. Solar Terr. Phys. 136, 174–186. https://doi.org/10.1016/j.jastp.2015.05.006.

Jarvis, M., 2009. Longitudinal variation in E- and F-region ionospheric trends. J. Atmos. Solar Terr. Phys. 71 (13), 1415–1429. https://doi.org/10.1016/j.jastp.2008.05.017.

Kalicinsky, C., Knieling, P., Koppmann, R., et al., 2016. Long-term dynamics of OH^* temperatures over central europe: trends and solar correlations. Atmos. Chem. Phys. 16 (23), 15033–15047. https://doi.org/10.5194/acp-16-15033-2016.

Keating, G.M., Tolson, R.H., Bradford, M.S., 2000. Evidence of long term global decline in the Earth's thermospheric densities apparently related to anthropogenic effects. Geophys. Res. Lett. 27 (10), 1523–1526. https://doi.org/10.1029/2000gl003771.

Kishore, P., Ratnam, M.V., Velicogna, I., et al., 2014. Long-term trends observed in the middle atmosphere temperatures using ground based LIDARs and satellite borne measurements. Ann. Geophys. 32 (3), 301–317. https://doi.org/10.5194/angeo-32-301-2014.

Laštovička, J., 2017. A review of recent progress in trends in the upper atmosphere. J. Atmos. Solar Terr. Phys. 163, 2–13. https://doi.org/10.1016/j.jastp.2017.03.009.

Laštovička, J., 2019. Is the relation between ionospheric parameters and solar proxies stable? Geophys. Res. Lett. 46 (24), 14208–14213. https://doi.org/10.1029/2019gl085033.

Laštovička, J., 2021a. The best solar activity proxy for long-term ionospheric investigations. Adv. Space Res. 68 (6), 2354–2360. https://doi.org/10.1016/j.asr.2021.06.032.

Laštovička, J., 2021b. What is the optimum solar proxy for long-term ionospheric investigations? Adv. Space Res. 67 (1), 2–8. https://doi.org/10.1016/j.asr.2020.07.025.

Laštovička, J., 2022. Long-term changes in ionospheric climate in terms of foF2. Atmosphere 13 (1), 110. https://doi.org/10.3390/atmos13010110.

Laštovička, J., 2024. Dependence of long-term trends in foF2 at middle latitudes on different solar activity proxies. Adv. Space Res. 73 (1), 685–689. https://doi.org/10.1016/j.asr.2023.09.047.

Laštovička, J., Akmaev, R.A., Beig, G., et al., 2006a. Global change in the upper atmosphere. Science 314 (5803), 1253–1254. https://doi.org/10.1126/science.1135134.

Laštovička, J., Bremer, J., 2004. An overview of long-term trends in the lower ionosphere below 120 km. Surv. Geophys. 25 (1), 69–99. https://doi.org/10.1023/b:geop.0000015388.75164.e2.

Laštovička, J., Burešová, D., Kouba, D., et al., 2016. Stability of solar correction for calculating ionospheric trends. Ann. Geophys. 34 (12), 1191–1196. https://doi.org/10.5194/angeo-34-1191-2016.

Laštovička, J., Jelínek, Š., 2019. Problems in calculating long-term trends in the upper atmosphere. J. Atmos. Solar Terr. Phys. 189, 80–86. https://doi.org/10.1016/j.jastp.2019.04.011.

Laštovička, J., Mikhailov, A., Ulich, T., et al., 2006. Long-term trends in foF2: A comparison of various methods. J. Atmos. Solar Terr. Phys. 68 (17), 1854–1870. https://doi.org/10.1016/j.jastp.2006.02.009.

Laštovička, J., Urbar, J., Kozubek, M., 2017. Long-term trends in the total electron content. Geophys. Res. Lett. 44 (16), 8168–8172. https://doi.org/10.1002/2017gl075063.

Lean, J.L., Emmert, J.T., Picone, J.M., et al., 2011. Global and regional trends in ionospheric total electron content. J. Geophys. Res.: Space Phys. 116 (A2). https://doi.org/10.1029/2010ja016378.

Lean, J.L., Meier, R.R., Picone, J.M., et al., 2016. Ionospheric total electron content: Spatial patterns of variability. J. Geophys. Res.: Space Phys. 121 (10). https://doi.org/10.1002/2016ja023210.

Lewis, H.G., Saunders, A., Swinerd, G., et al., 2011. Effect of thermospheric contraction on remediation of the near-Earth space debris environment. J. Geophys. Res.: Space Phys. 116 (A2). https://doi.org/10.1029/2011ja016482.

Li, T., Leblanc, T., McDermid, I.S., et al., 2011. Middle atmosphere temperature trend and solar cycle revealed by long-term Rayleigh lidar observations. J. Geophys. Res. 116. https://doi.org/10.1029/2010jd015275.

Li, T., Yue, J., Russell, J.M., et al., 2021. Long-term trend and solar cycle in the middle atmosphere temperature revealed from merged HALOE and SABER datasets. J. Atmos. Solar Terr. Phys. 212, 105506. https://doi.org/10.1016/j.jastp.2020.105506.

Lin, C.Y., Deng, Y., 2019. Nitric oxide in climatological global energy budget during 1982–2013. J. Geophys. Res.: Space Phys. 124 (1), 782–789. https://doi.org/10.1029/2018ja025902.

Liu, X., Xu, J., Yue, J., et al., 2024. Trends in the high-latitude mesosphere temperature and mesopause revealed by SABER. Atmos. Chem. Phys. 24 (17), 10143–10157. https://doi.org/10.5194/acp-24-10143-2024.

Liu, X., Yue, J., Xu, J., et al., 2017. Variations of global gravity waves derived from 14 years of SABER temperature observations. J. Geophys. Res.: Atmos. 122 (12), 6231–6249. https://doi.org/10.1002/2017jd026604.

Lockwood, M., 2010. Solar change and climate: an update in the light of the current exceptional solar minimum. Proc. Roy. Soc. A: Math., Phys. Eng. Sci. 466 (2114), 303–329. https://doi.org/10.1098/rspa.2009.0519.

Lockwood, M., Stamper, R., Wild, M.N., 1999. A doubling of the Sun's coronal magnetic field during the past 100 years. Nature 399 (6735), 437–439. https://doi.org/10.1038/20867.

Loeb, N.G., Wielicki, B.A., Wong, T., et al., 2009. Impact of data gaps on satellite broadband radiation records. J. Geophys. Res.: Atmos. 114 (D11). https://doi.org/10.1029/2008jd011183.

Lukianova, R., Mursula, K., 2011. Changed relation between sunspot numbers, solar UV/EUV radiation and TSI during the declining phase of solar cycle 23. J. Atmos. Solar Terr. Phys. 73 (2–3), 235–240. https://doi.org/10.1016/j.jastp.2010.04.002.

Lübken, F.-J., Berger, U., Baumgarten, G., 2013. Temperature trends in the midlatitude summer mesosphere. J. Geophys. Res.: Atmos. 118 (24), 13347–13360. https://doi.org/10.1002/2013jd020576.

Manabe, S., Wetherald, R.T., 1967. Thermal equilibrium of the atmosphere with a given distribution of relative humidity. Journal of the Atmospheric Sciences 24 (3), 241–259. https://doi.org/10.1175/1520-0469(1967)024<0241:teotaw>2.0.co;2.

Manabe, S., Wetherald, R.T., 1975. The effects of doubling the CO_2 concentration on the climate of a general circulation model. Journal of the Atmospheric Sciences 32 (1), 3–15. https://doi.org/10.1175/1520-0469(1975)032<0003:teodtc>2.0.co;2.

Marcos, F.A., Wise, J.O., Kendra, M.J., et al., 2005. Detection of a long-term decrease in thermospheric neutral density. Geophys. Res. Lett. 32 (4). https://doi.org/10.1029/2004gl021269, n/a–n/a.

Marin, D., Mikhailov, A.V., Morena, B.A., et al., 2001. Long-term hmF2 trends in the Eurasian longitudinal sector from the ground-based ionosonde observations. Ann. Geophys. 19 (7), 761–772. https://doi.org/10.5194/angeo-19-761-2001.

Matthes, K., Funke, B., Andersson, M.E., et al., 2017. Solar forcing for CMIP6 (v3.2). Geoscientific Model Development 10 (6), 2247–2302. https://doi.org/10.5194/gmd-10-2247-2017.

Matzka, J., Siddiqui, T.A., Lilienkamp, H., et al., 2017. Quantifying solar flux and geomagnetic main field influence on the equatorial ionospheric current system at the geomagnetic observatory Huancayo. J. Atmos. Solar Terr. Phys. 163, 120–125. https://doi.org/10.1016/j.jastp.2017.04.014.

McInerney, J.M., Qian, L., Liu, H., et al., 2024. Climate change in the thermosphere and ionosphere from the early twentieth century to early twenty-first century simulated by the Whole Atmosphere Community Climate Model—eXtended. J. Geophys. Res.: Atmos. 129 (3). https://doi.org/10.1029/2023jd039397.

Meinshausen, M., Smith, S.J., Calvin, K., et al., 2011. The rcp greenhouse gas concentrations and their extensions from 1765 to 2300. Climatic Change 109 (1–2), 213–241. https://doi.org/10.1007/s10584-011-0156-z.

Mielich, J., Bremer, J., 2013. Long-term trends in the ionospheric F2 region with different solar activity indices. Ann. Geophys. 31 (2), 291–303. https://doi.org/10.5194/angeo-31-291-2013.

Mikhailov, A.V., 2006. Ionospheric long-term trends: can the geomagnetic control and the greenhouse hypotheses be reconciled? Ann. Geophys. 24 (10), 2533–2541. https://doi.org/10.5194/angeo-24-2533-2006.

Mikhailov, A.V., de la Morena, B.A., 2003. Long-term trends of $f_o e$ and geomagnetic activity variations. Ann. Geophys. 21 (3), 751–760. https://doi.org/10.5194/angeo-21-751-2003.

Mikhailov, A.V., Perrone, L., Nusinov, A.A., 2017. A mechanism of midlatitude noontime $f_o e$ long-term variations inferred from European observations. J. Geophys. Res.: Space Phys. 122 (4), 4466–4473. https://doi.org/10.1002/2017ja023909.

Mlynczak, M., Yue, J., McCormack, J., et al., 2021. An observational gap at the edge of space. Eos 102. https://doi.org/10.1029/2021eo155494.

Mlynczak, M.G., Hunt, L.A., Garcia, R., et al., 2024. Energy conservation in the cooling and contracting upper mesosphere and lower thermosphere. Geophys. Res. Lett. 51 (14). https://doi.org/10.1029/2024gl109757.

Mlynczak, M.G., Hunt, L.A., Garcia, R.R., et al., 2022. Cooling and contraction of the mesosphere and lower thermosphere. J. Geophys. Res.: Atmos. 127 (22). https://doi.org/10.1029/2022jd036767, from 2002 to 2021.

Mlynczak, M.G., Hunt, L.A., Marshall, B.T., et al., 2010. Observations of infrared radiative cooling in the thermosphere on daily to multiyear timescales from the TIMED/SABER instrument. J. Geophys. Res.: Space Phys. 115 (A3), A03309. https://doi.org/10.1029/2009ja014713.

Mlynczak, M.G., Knipp, D.J., Hunt, L.A., et al., 2018. Space-based sentinels for measurement of infrared cooling in the thermosphere for space weather nowcasting and forecasting. Space Weather 16 (4), 363–375. https://doi.org/10.1002/2017sw001757.

Mursula, K., Pevtsov, A.A., Asikainen, T., et al., 2024. Transition to a weaker Sun: Changes in the solar atmosphere during the decay of the Modern Maximum. Astronomy & Astrophysics 685, A170. https://doi.org/10.1051/0004-6361/202449231.

Offermann, D., Hoffmann, P., Knieling, P., et al., 2010. Long-term trends and solar cycle variations of mesospheric temperature and dynamics. J. Geophys. Res. 115 (D18). https://doi.org/10.1029/2009jd013363.

Ogawa, Y., Motoba, T., Buchert, S.C., et al., 2014. Upper atmosphere cooling over the past 33 years. Geophys. Res. Lett. 41 (15), 5629–5635. https://doi.org/10.1002/2014gl060591.

Oliver, W.L., Holt, J.M., Zhang, S.-R., et al., 2014. Long-term trends in thermospheric neutral temperature and density above millstone hill. J.

Geophys. Res.: Space Phys. 119 (9), 7940–7946. https://doi.org/10.1002/2014ja020311.
Oliver, W.L., Zhang, S.-R., Goncharenko, L.P., 2013. Is thermospheric global cooling caused by gravity waves? J. Geophys. Res.: Space Phys. 118 (6), 3898–3908. https://doi.org/10.1002/jgra.50370.
O'Neill, B.C., Tebaldi, C., van Vuuren, D.P., et al., 2016. The scenario model intercomparison project (ScenarioMIP) for CMIP6. Geoscientific Model Development 9 (9), 3461–3482. https://doi.org/10.5194/gmd-9-3461-2016.
Picone, J.M., Hedin, A.E., Drob, D.P., et al., 2002. NRLMSISE-00 empirical model of the atmosphere: Statistical comparisons and scientific issues. J. Geophys. Res.: Space Phys. 107 (A12), SIA 15-1–SIA 15-16. https://doi.org/10.1029/2002ja009430.
Portmann, R.W., Thomas, G.E., Solomon, S., et al., 1995. The importance of dynamical feedbacks on doubled co2-induced changes in the thermal structure of the mesosphere. Geophys. Res. Lett. 22 (13), 1733–1736. https://doi.org/10.1029/95gl01432.
Pramitha, M., Kishore Kumar, K., Praveen, M., 2023. Long-term variabilities in thermal structure, CO_2 concentration and associated cooling rates in the Earth's middle atmosphere: Observations and model simulations. J. Atmos. Solar Terr. Phys. 246, 106070. https://doi.org/10.1016/j.jastp.2023.106070.
Qian, L., Burns, A.G., Solomon, S.C., et al., 2009. The effect of carbon dioxide cooling on trends in the F2-layer ionosphere. J. Atmos. Solar Terr. Phys. 71 (14–15), 1592–1601. https://doi.org/10.1016/j.jastp.2009.03.006.
Qian, L., Burns, A.G., Solomon, S.C., et al., 2017. Carbon dioxide trends in the mesosphere and lower thermosphere. J. Geophys. Res.: Space Phys. 122 (4), 4474–4488. https://doi.org/10.1002/2016ja023825.
Qian, L., Laštovička, J., Roble, R.G., et al., 2011. Progress in observations and simulations of global change in the upper atmosphere. J. Geophys. Res.: Space Phys. 116 (A2). https://doi.org/10.1029/2010ja016317.
Qian, L., Marsh, D., Merkel, A., et al., 2013. Effect of trends of middle atmosphere gases on the mesosphere and thermosphere. J. Geophys. Res.: Space Phys. 118 (6), 3846–3855. https://doi.org/10.1002/jgra.50354.
Qian, L., McInerney, J.M., Solomon, S.S., et al., 2021. Climate changes in the upper atmosphere: Contributions by the changing greenhouse gas concentrations and Earth's magnetic field from the 1960s to 2010s. J. Geophys. Res.: Space Phys. 126 (3). https://doi.org/10.1029/2020ja029067.
Qian, L., Roble, R.G., Solomon, S.C., et al., 2006. Calculated and observed climate change in the thermosphere, and a prediction for solar cycle 24. Geophys. Res. Lett. 33 (23). https://doi.org/10.1029/2006gl027185.
Qian, L., Solomon, S.C., Roble, R.G., 2014. Secular changes in the thermosphere and ionosphere between two quiet Sun periods. J. Geophys. Res.: Space Phys. 119 (3), 2255–2262. https://doi.org/10.1002/2013ja019438.
Ramesh, K., Smith, A.K., Garcia, R.R., et al., 2020. Long-term variability and tendencies in middle atmosphere temperature and zonal wind from WACCM6 simulations during 1850–2014. J. Geophys. Res.: Atmos. 125 (24). https://doi.org/10.1029/2020jd033579.
Ratnam, M.V., Kumar, G.K., Rao, N.V., et al., 2013. Evidence of long-term change in zonal wind in the tropical lower mesosphere: Observations and model simulations. Geophys. Res. Lett. 40 (2), 397–401. https://doi.org/10.1002/grl.50158.
Ratnam, M.V., Raj, S.A., Qian, L., 2019. Long-term trends in the low-latitude middle atmosphere temperature and winds: Observations and WACCM-x model simulations. J. Geophys. Res.: Space Phys. 124 (8), 7320–7331. https://doi.org/10.1029/2019ja026928.
Rezac, L., Yue, J., Yongxiao, J., et al., 2018. On long-term SABER CO_2 trends and effects due to nonuniform space and time sampling. J. Geophys. Res.: Space Phys. 123 (9), 7958–7967. https://doi.org/10.1029/2018ja025892.
Rishbeth, H., 1990. A greenhouse effect in the ionosphere? Planet. Space Sci. 38 (7), 945–948. https://doi.org/10.1016/0032-0633(90)90061-t.
Rishbeth, H., Roble, R., 1992. Cooling of the upper atmosphere by enhanced greenhouse gases — modelling of thermospheric and ionospheric effects. Planet. Space Sci. 40 (7), 1011–1026. https://doi.org/10.1016/0032-0633(92)90141-a.
Roble, R.G., 1995. Energetics of the mesosphere and thermosphere. In: Johnson, R., Killeen, T. (Eds.), The Upper Mesosphere and Lower Thermosphere: A Review of Experiment and Theory. American Geophysical Union, pp. 1–21. https://doi.org/10.1029/gm087p0001.
Roble, R.G., Dickinson, R.E., 1989. How will changes in carbon dioxide and methane modify the mean structure of the mesosphere and thermosphere? Geophys. Res. Lett. 16 (12), 1441–1444. https://doi.org/10.1029/gl016i012p01441.
Russell, C.T., Luhmann, J.G., Jian, L.K., 2010. How unprecedented a solar minimum? Rev. Geophys. 48 (2). https://doi.org/10.1029/2009rg000316.
Saunders, A., Lewis, H., Swinerd, G., 2011. Further evidence of long-term thermospheric density change using a new method of satellite ballistic coefficient estimation. J. Geophys. Res.: Space Phys. 116 (A2). https://doi.org/10.1029/2010ja016358, n/a–n/a.
Scharroo, R., Smith, W.H.F., 2010. A global positioning system-based climatology for the total electron content in the ionosphere. J. Geophys. Res.: Space Phys. 115 (A10). https://doi.org/10.1029/2009ja014719.
Schmidt, H., Brasseur, G.P., Charron, M., et al., 2006. The HAMMONIA chemistry climate model: Sensitivity of the mesopause region to the 11-year solar cycle and CO_2 doubling. J. Clim. 19 (16), 3903–3931. https://doi.org/10.1175/jcli3829.1.
Schunk, R.W., Nagy, A.F., 2000. Ionospheres. Cambridge University Press. https://doi.org/10.1017/cbo9780511551772.
Selvaraj, D., Sulzer, M.P., Zhang, S., et al., 2023. Long-term trends in the upper atmosphere using the incoherent scatter radar observations over Arecibo. J. Geophys. Res.: Space Phys. 128 (2). https://doi.org/10.1029/2022ja031049.
She, C.-Y., Berger, U., Yan, Z.-A., et al., 2019. Solar response and long-term trend of midlatitude mesopause region temperature based on 28 years (1990–2017) of Na lidar observations. J. Geophys. Res.: Space Phys. 124 (8), 7140–7156. https://doi.org/10.1029/2019ja026759.
Shinbori, A., Koyama, Y., Nose, M., et al., 2014. Long-term variation in the upper atmosphere as seen in the geomagnetic solar quiet daily variation. Earth, Planets and Space 66 (1). https://doi.org/10.1186/s40623-014-0155-1.
Shutler, J.D., Yan, X., Cnossen, I., et al., 2022. Atmospheric impacts of the space industry require oversight. Nat. Geosci. 15 (8), 598–600. https://doi.org/10.1038/s41561-022-01001-5.
Slominska, E., Strumik, M., Slominski, J., et al., 2020. Analysis of the impact of long-term changes in the geomagnetic field on the spatial pattern of the Weddell Sea anomaly. J. Geophys. Res.: Space Phys. 125 (5). https://doi.org/10.1029/2019ja027528.
Soares, G., Yamazaki, Y., Cnossen, I., et al., 2020. Evolution of the geomagnetic daily variation at Tatuoca, Brazil, from 1957 to 2019: A transition from Sq to EEJ. J. Geophys. Res.: Space Phys. 125 (9). https://doi.org/10.1029/2020ja028109.
Solomon, S.C., Liu, H.-L., Marsh, D.R., et al., 2018. Whole atmosphere simulation of anthropogenic climate change. Geophys. Res. Lett. 45 (3), 1567–1576. https://doi.org/10.1002/2017gl076950.
Solomon, S.C., Liu, H.-L., Marsh, D.R. et al. (2019). Whole atmosphere climate change: Dependence on solar activity. J. Geophys. Res.: Space Phys., doi:10.1029/2019ja026678.
Solomon, S.C., Qian, L., Burns, A.G., 2013. The anomalous ionosphere between solar cycles 23 and 24. J. Geophys. Res.: Space Phys. 118 (10), 6524–6535. https://doi.org/10.1002/jgra.50561.
Solomon, S.C., Qian, L., Roble, R.G., 2015. New 3-d simulations of climate change in the thermosphere. J. Geophys. Res.: Space Phys. 120 (3), 2183–2193. https://doi.org/10.1002/2014ja020886.
Stamper, R., Lockwood, M., Wild, M.N., et al., 1999. Solar causes of the long-term increase in geomagnetic activity. J. Geophys. Res.: Space Phys. 104 (A12), 28325–28342. https://doi.org/10.1029/1999ja900311.

Takeda, M., 1996. Effects of the strength of the geomagnetic main field strength on the dynamo action in the ionosphere. J. Geophys. Res.: Space Phys. 101 (A4), 7875–7880. https://doi.org/10.1029/95ja03807.

Tao, C., Jin, H., Shinagawa, H., et al., 2017. Effect of intrinsic magnetic field decrease on the low- to middle-latitude upper atmosphere dynamics simulated by GAIA. J. Geophys. Res.: Space Phys. 122 (9), 9751–9762. https://doi.org/10.1002/2017ja024278.

Thu, H.P.T., Amory-Mazaudier, C., Huy, M.L., et al., 2016. f_oF_2 long-term trend linked to Earth's magnetic field secular variation at a station under the northern crest of the equatorial ionization anomaly. J. Geophys. Res.: Space Phys. 121 (1), 719–726. https://doi.org/10.1002/2015ja021890.

Upadhyay, H.O., Mahajan, K.K., 1998. Atmospheric greenhouse effect and ionospheric trends. Geophys. Res. Lett. 25 (17), 3375–3378. https://doi.org/10.1029/98gl02503.

van Vuuren, D.P., Edmonds, J., Kainuma, M., et al., 2011. The representative concentration pathways: an overview. Climatic Change 109 (1–2), 5–31. https://doi.org/10.1007/s10584-011-0148-z.

Wang, H., Gao, J., Zhang, K., 2022. Influence of the magnetic field strength and solar activity on the thermospheric zonal wind. J. Geophys. Res.: Space Phys. 127 (1). https://doi.org/10.1029/2021ja029741.

Wang, H., Zhang, J., Lühr, H., et al., 2017. Longitudinal modulation of electron and mass densities at middle and auroral latitudes: Effect of geomagnetic field strength. J. Geophys. Res.: Space Phys. 122 (6), 6595–6610. https://doi.org/10.1002/2016ja023829.

Weber, M., Arosio, C., Coldewey-Egbers, M., et al., 2022. Global total ozone recovery trends attributed to ozone-depleting substance ODS changes derived from five merged ozone datasets. Atmos. Chem. Phys. 22 (10), 6843–6859. https://doi.org/10.5194/acp-22-6843-2022.

Weng, L., Lei, J., Zhong, J., et al., 2020. A machine-learning approach to derive long-term trends of thermospheric density. Geophys. Res. Lett. 47 (6). https://doi.org/10.1029/2020gl087140.

Wilhelm, S., Stober, G., Brown, P., 2019. Climatologies and long-term changes in mesospheric wind and wave measurements based on radar observations at high and mid latitudes. Ann. Geophys. 37 (5), 851–875. https://doi.org/10.5194/angeo-37-851-2019.

Dudok de Wit, T., Bruinsma, S., 2017. The 30 cm radio flux as a solar proxy for thermosphere density modelling. J. Space Weather Space Clim. 7, A9. https://doi.org/10.1051/swsc/2017008.

Yuan, T., Solomon, S.C., She, C.-Y., et al., 2019. The long-term trends of nocturnal mesopause temperature and altitude revealed by Na lidar observations between 1990 and 2018 at midlatitude. J. Geophys. Res.: Atmos. 124 (12), 5970–5980. https://doi.org/10.1029/2018jd029828.

Yue, J., Russell, J., Jian, Y., et al., 2015. Increasing carbon dioxide concentration in the upper atmosphere observed by SABER. Geophys. Res. Lett. 42 (17), 7194–7199. https://doi.org/10.1002/2015gl064696.

Yue, X., Hu, L., Wei, Y., et al., 2018. Ionospheric trend over Wuhan during 1947–2017: Comparison between simulation and observation. J. Geophys. Res.: Space Phys. 123 (2), 1396–1409. https://doi.org/10.1002/2017ja024675.

Yue, X., Liu, L., Wan, W., et al., 2008. Modeling the effects of secular variation of geomagnetic field orientation on the ionospheric long term trend over the past century. J. Geophys. Res.: Space Phys. 113 (A10). https://doi.org/10.1029/2007ja012995.

Yue, X., Wan, W., Liu, L., et al., 2006. Applying artificial neural network to derive long-term foF2 trends in the Asia/Pacific sector from ionosonde observations. J. Geophys. Res. 111 (A10). https://doi.org/10.1029/2005ja011577.

Zhang, S.-R., Cnossen, I., Laštovicka, J., et al., 2023. Long-term geospace climate monitoring. Front. Astron. Space Sci. 10. https://doi.org/10.3389/fspas.2023.1139230.

Zhang, S.-R., Holt, J.M., 2013. Long-term ionospheric cooling: Dependency on local time, season, solar activity, and geomagnetic activity. J. Geophys. Res.: Space Phys. 118 (6), 3719–3730. https://doi.org/10.1002/jgra.50306.

Zhang, S.-R., Holt, J.M., Erickson, P.J., et al., 2016. Ionospheric ion temperature climate and upper atmospheric long-term cooling. J. Geophys. Res.: Space Phys. 121 (9), 8951–8968. https://doi.org/10.1002/2016ja022971.

Zhang, S.-R., Holt, J.M., Kurdzo, J., 2011. Millstone Hill ISR observations of upper atmospheric long-term changes: Height dependency. J. Geophys. Res.: Space Phys. 116 (A2). https://doi.org/10.1029/2010ja016414.

Zhao, X.R., Sheng, Z., Shi, H.Q., et al., 2021. Middle atmosphere temperature changes derived from SABER observations during 2002–2020. J. Clim., 1 https://doi.org/10.1175/jcli-d-20-1010.1.

Zhao, X.R., Sheng, Z., Shi, H.Q., et al., 2020. Long-term trends and solar responses of the mesopause temperatures observed by SABER during the 2002–2019 period. J. Geophys. Res.: Atmos. 125 (11). https://doi.org/10.1029/2020jd032418.

Zossi, B.S., Elias, A.G., Fagre, M., 2018. Ionospheric conductance spatial distribution during geomagnetic field reversals. J. Geophys. Res.: Space Phys., doi:10.1002/2017ja024925.